

AD-A185 471

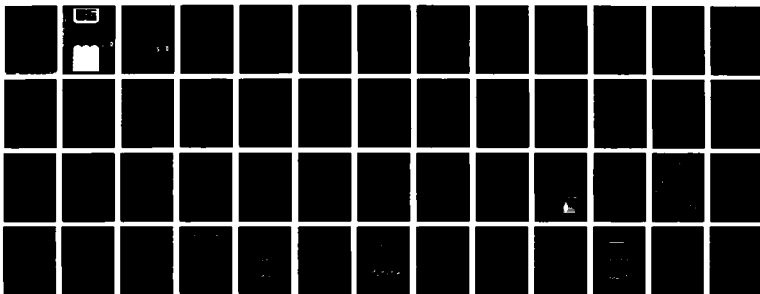
NATURE AND THE NONLINEAR EVOLUTION OF ELECTROSTATIC
WAVES ASSOCIATED WITH.. (U) IOWA UNIV IOWA CITY DEPT OF
PHYSICS AND ASTRONOMY N OMIDI ET AL. JUL 87

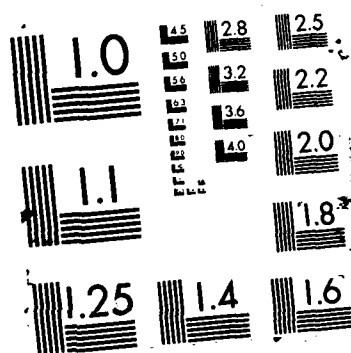
1/1

UNCLASSIFIED N00014-82-K-0103

F/G 3/2

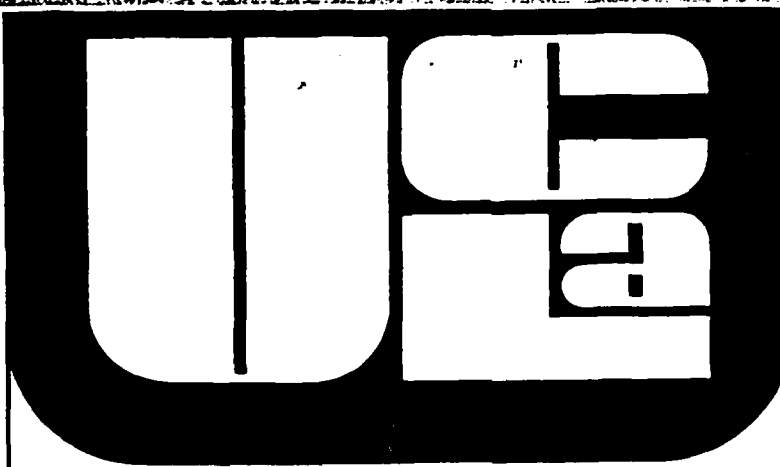
NL





NTIC FILE COPY

AD-A185 471



12

NATURE AND THE NONLINEAR EVOLUTION OF ELECTROSTATIC
WAVES ASSOCIATED WITH THE AMPTE SOLAR WIND RELEASES

N. Omidi¹, K. Akimoto², D.A. Gurnett³, and R.R. Anderson³

July 1987

PPG-1083

IGPP-3042

DTIC
ELECTE
OCT 26 1987
S D

CENTER FOR
PLASMA PHYSICS
AND
FUSION ENGINEERING
UNIVERSITY OF CALIFORNIA
LOS ANGELES

DISTRIBUTION STATEMENT A
Approved for public release;
Distribution Unlimited

87 10 19 10

12

NATURE AND THE NONLINEAR EVOLUTION OF ELECTROSTATIC
WAVES ASSOCIATED WITH THE AMPTE SOLAR WIND RELEASES

N. Omidi¹, K. Akimoto², D.A. Gurnett³, and R.R. Anderson³

July 1987

PPG-1083

JGPP-3042

1 ^{univ. 1} ~~Institute~~ of Geophysics and Planetary Physics ^{✓ 2nd}
~~University of California, Los Angeles~~
Los Angeles, CA 90024-1567

2 Earth and Space Sciences Division and
Applied Theoretical Physics Division
Los Alamos National Laboratory
Los Alamos, NM 87545

3 Department of Physics and Astronomy
The University of Iowa
Iowa City, IA 52242

DTIC
ELECTE
OCT 26 1987
S D
ce

DISTRIBUTION STATEMENT 1

Approved for public release
Distribution Unlimited

Unclassified

SECURITY CLASSIFICATION OF THIS PAGE (When Data Entered)

REPORT DOCUMENTATION PAGE		READ INSTRUCTIONS BEFORE COMPLETING FORM
1. REPORT NUMBER None	2. GOVT ACCESSION NO. ADA185 471	3. RECIPIENT'S CATALOG NUMBER
4. TITLE (and Subtitle) Nature and the Nonlinear Evolution of Electrostatic Waves Associated with the AMPTE Solar Wind Releases		5. TYPE OF REPORT & PERIOD COVERED Progress July 1987
7. AUTHOR(s) N. Omid, K. Akimoto, D. A. Gurnett and R. R. Anderson		6. PERFORMING ORG. REPORT NUMBER
9. PERFORMING ORGANIZATION NAME AND ADDRESS The University of Iowa Dept. of Physics and Astronomy Iowa City, IA 52242		8. CONTRACT OR GRANT NUMBER(s) N00014-82-K-0183
11. CONTROLLING OFFICE NAME AND ADDRESS Electronics Program Office Office of Naval Research Arlington, VA 22217		10. PROGRAM ELEMENT, PROJECT, TASK AREA & WORK UNIT NUMBERS
14. MONITORING AGENCY NAME & ADDRESS (if different from Controlling Office)		12. REPORT DATE July 1987
		13. NUMBER OF PAGES 51
		15. SECURITY CLASS. (of this report) UNCLASSIFIED
		15a. DECLASSIFICATION/DOWNGRADING SCHEDULE
16. DISTRIBUTION STATEMENT (of this Report) Approved for public release; distribution is unlimited.		
17. DISTRIBUTION STATEMENT (of the abstract entered in Block 20, if different from Report)		
18. SUPPLEMENTARY NOTES		
19. KEY WORDS (Continue on reverse side if necessary and identify by block number) AMPTE Electrostatic waves Solar wind releases		
20. ABSTRACT (Continue on reverse side if necessary and identify by block number) (See following page)		

NATURE AND THE NONLINEAR EVOLUTION OF ELECTROSTATIC WAVES
ASSOCIATED WITH THE AMPTE SOLAR WIND RELEASES

N. Omid¹, K. Akimoto², D.A. Gurnett³, and R.R. Anderson³

¹Institute of Geophysics and Planetary Physics
University of California, Los Angeles
Los Angeles, California 90024

²Earth and Space Sciences Division and
Applied Theoretical Physics Division
Los Alamos National Laboratory
Los Alamos, New Mexico 87545



³Department of Physics and Astronomy
The University of Iowa
Iowa City, Iowa 52242

July, 1987

Accession For	
NTIS CRA&I	<input checked="checked" type="checkbox"/>
DTIC TAB	<input type="checkbox"/>
Unannounced	<input type="checkbox"/>
Justification	
By	
Distribution/	
Availability Codes	
Dist	Avail and/or Special
A-1	

ABSTRACT

To understand the generation and the nonlinear evolution of the electrostatic waves observed during the AMPTE (Active Magnetosphere Particle Tracer Explorers) solar wind releases ¹⁵ ~~a detailed~~ ^{ed.} investigation ^{is} conducted. Previous linear studies ~~have indicated that~~ two distinct sets of instabilities may be responsible for the generation ~~of these waves~~. One set consists of ion-acoustic type instabilities which are insensitive to the presence of a background magnetic field, while the other group corresponds to the modified two stream instabilities and requires the solar wind flow to be across the ambient magnetic field. ~~In order~~ ² to establish which set of instabilities ¹⁵ ~~are~~ more viable for the generation of the observed electrostatic waves ¹⁵ a detailed linear Vlasov theory has been conducted by numerically solving the full electromagnetic dispersion relation. In addition both the plasma wave as well as the magnetic field measurements by the IRM (Ion Release Module) spacecraft were used to correlate the frequency and the power of the observed waves with the magnitude and the direction of the solar wind magnetic field. The results of these analyses indicate that the ion-acoustic type instabilities have growth rates that are an order of magnitude or more larger than those of the modified two stream instabilities. Similarly the observations show no correlation between the magnitude and the direction of the ambient magnetic field on the one hand, and the wave frequency and amplitude on the other hand, thus, indicating that the ion-acoustic type instabilities are the likely generation mechanism. In order to investigate the nonlinear evolution of these instabilities, and discern their role in the coupling of the released ions to the solar wind, one-dimensional electrostatic simulations have been performed. The results show that both the solar wind protons and the released ions may be heated and accelerated in the directions oblique to the solar wind flow velocity.

1. INTRODUCTION

One of the interesting and fundamental problems in the field of space plasma physics is the collisionless interaction between a flowing plasma and newly created ions due to ionization of neutral gases. This type of a problem can be present under a variety of physical settings such as during the interaction between the solar wind and comets or interstellar helium gas. Similarly, there have been a number of active experiments in space in which understanding of the interaction between the background plasma and the newly ionized gases has been a primary concern. Among these are the experiments conducted during the AMPTE (Active Magnetospheric Particle Tracer Explorers) mission in which lithium or barium gasses were released in both the solar wind and the magnetosphere. One of the main objectives of these experiments was to trace the motion of the released ions and thereby learn more about the transport properties of the solar wind and the magnetosphere. Clearly, since both the released ions and the background plasma were collisionless, any interaction between the two must have taken place through the electromagnetic forces which were present in the medium prior to the release as well as those that were generated after the release due to collective plasma processes. Thus, in order to gain an understanding of the particle motion, it is necessary to investigate the role of collective plasma processes. In this study, the role of wave particle interactions during the AMPTE solar wind releases is investigated.

During the AMPTE mission, four releases were made in the solar wind. Of these four, two were lithium releases which took place on September 11 and 20, 1984; and two were barium releases which took place on December 27, 1984, and July 18, 1985. During all of these releases, intense bursts of electrostatic noise were observed on the upstream side of the ion cloud outside of the diamagnetic cavity [Gurnett et al., 1985; Häusler et al., 1986; Gurnett et al., 1986a,b]. These

waves ranged in frequency between tens of Hz to several KHz and their peak integrated electric field strength was as high as 40 mV/m. An example of these waves is given in the bottom panel of Figure 1. In this panel the electric field intensities measured by the plasma wave instrument on board the AMPTE/IRM (Ion Release Module) spacecraft during the September 11 lithium release are shown. In this spectrogram, the axis of ordinates corresponds to 16 frequency channels ranging from 31.1 Hz to 178 KHz, while the axis of abscissas shows Universal Time (UT). The top three panels in Figure 1 show the magnetic field measurements in geocentric solar ecliptic (GSE) coordinates during the same time period [Lühr et al., 1986]. As can be seen in the third panel the magnetic field strength falls from its solar wind value (~ 6 nT) to nearly zero at 07:25:04 UT indicating the entrance of the IRM spacecraft into the diamagnetic cavity formed by the lithium cloud. As this cloud passes the spacecraft, the magnetic field begins to rise at about 07:25:15 UT reaching values as high as 23nT. This region of enhanced magnetic field corresponds to a pile up region upstream of the lithium cloud (for a more detailed description of the data see Gurnett et al., 1986a and Lühr et al., 1986). The onset of intense electrostatic waves can be seen in the bottom panel at about 07:25:30 UT reaching peak power at 07:25:35 UT. As has been shown by Gurnett et al. (1985, 1986a) and illustrated in more detail later in this paper the spectrum of these waves peaks at frequencies between a hundred and a few hundred Hertz.

In order to understand the generation mechanism of the observed electrostatic noise a number of linear studies have been performed [Gurnett et al., 1986a,b; Brinca et al., 1986; Papadopoulos et al., 1987; Ma et al., 1987]. In Gurnett et al. (1986a,b) it was suggested that the wave amplification takes place via an ion-acoustic type instability due to the relative drift between the solar wind and the newly created ions. In these studies growth rates of the waves with phase velocity along the solar wind flow were calculated and shown to be significant. These studies were later

extended to obliquely propagating waves showing that the growth rates of these waves are comparable or larger than the parallel propagating waves [Brinca et al., 1986; Ma et al., 1987]. Specifically, it was shown by Ma et al. (1987) that two types of instabilities are possible. One is an instability due to the relative drift between the released ions and all the electrons, while the other is due to the streaming between the released ions and the solar wind protons. Both of these instabilities, however, are ion-acoustic type in that the wave dispersion properties are similar to that of ion-acoustic waves. In fact using the nomenclature used by Gary and Omidi (1987), the first type of instability corresponds to the electron/ion-acoustic, while the second one corresponds to the ion/ion-acoustic instabilities. Of primary importance is the fact that these two instabilities are insensitive to the presence of a background magnetic field [Akimoto and Omidi, 1986; Gary and Omidi, 1987].

In addition to the above set of instabilities, another set has also been suggested by Papadopoulos et al. (1987) to be responsible for the generation of the electrostatic waves. These types of instabilities arise when a relative drift between the electrons and ions or two ion species exists across a magnetic field. In these instabilities, it is essential that the electrons be treated as magnetized while the ions may be considered as unmagnetized. Because the magnetic field in a plasma plays an important role for these modes, the parameter β (the ratio of kinetic to magnetic pressure) can greatly affect the growth rates of these waves. In fact while these waves are adequately described by the electrostatic dispersion relation at low values of β , electromagnetic effects become important as β increases, until eventually an electromagnetic dispersion relation must be used to discern their properties such as growth rates.

Although in general it is possible for all of the above mentioned instabilities to be operative simultaneously, it is much more likely that one of them becomes dominant and thereby governs the nature of the wave-particle interactions during the non-

linear regime. Because our main objective is to discern the role of the observed waves on particle dynamics, it is essential that the likely instability responsible for the generation of these waves be identified. This is the aim of the next section in which the growth rate calculations of Papadopoulos et al. (1987) will be extended by using the full electromagnetic dispersion relation. In addition, the plasma wave and the magnetic field measurements will be utilized to discern the role of the magnetic field magnitude and direction on the wave properties, and thereby deduce the nature of the instability. As will be shown in the next section the electron/ion-acoustic and the ion/ion-acoustic instabilities were more likely responsible for the generation of the electrostatic waves.

Having determined the nature of the instability in Section 2, a detailed simulation study will be conducted in Section 3 to discern the nonlinear evolution of the waves and thereby gain a better understanding of the wave-particle interactions during the AMPTE solar wind releases. The simulations consist of two parts; one in which the electrons and the ions are treated as particles with unrealistic mass ratios. The results of such a simulation study were briefly described by Omidi et al. (1987). The other type of simulation consists of fluid electrons and particle ions. The advantage of this kind of simulation method is that realistic mass ratios are used and thereby the observed plasma parameters can be utilized. A summary and discussion of the results will be presented in Section 4.

2. LINEAR ANALYSIS

2.1 Theory

As mentioned earlier one way in which the viability of the various proposed instabilities in generating the observed electrostatic noise can be tested is by comparing their linear growth rates. To do so we use a plasma model similar to that given by Gurnett et al. (1986a) in which the released ions (in this case lithium) form a cold non-drifting Maxwellian with a temperature $T_{Li} = 2 \times 10^3 \text{K}$. The solar wind protons form a Maxwellian with temperature $T_p = 10^5 \text{K}$ and a drift speed $V_{sw} = 450 \text{ km/s}$. As for the electrons two possibilities were allowed; in one case the electrons consisted of two separate Maxwellian populations with temperatures $T_e^h = 5 \times 10^5 \text{K}$ and $T_e^c = 5 \times 10^4 \text{K}$ corresponding to solar wind electrons and those associated with the photoionization of the released gas respectively. In the other case only the solar wind electrons were present allowing for the fact that the colder photoelectrons get replaced by the hotter solar wind electrons. In both cases the electrons were assumed to have a drift speed such that the net current was zero. It should, however, be mentioned that growth rate calculations with finite current in the plasma were also performed showing no significant difference in the results (see Gurnett et al., 1986a). Finally in regards to the density ratio of the released ions to the solar wind protons a wide range of values were considered. Observations show that the density ratio changes considerably with distance from the outer edge of the diamagnetic cavity. The results of linear theory have shown that the growth rates are maximum when the proton and the lithium (or barium) densities are equal. Throughout this paper, we take the density ratio to be one, because the role of this parameter is the same in both sets of instabilities.

Because the growth rate calculations of the ion-acoustic type instabilities have been performed in great detail in previous studies [Gurnett et al., 1986a,b; Brinca et

al., 1986; Ma et al., 1987], here we will only summarize the pertinent results. Figure 2 (from Ma et al., 1987) shows the growth rates (γ_{\max}) of electrostatic waves maximized over the wave number (K) as a function of θ (the angle between the \vec{K} vector and the solar wind velocity) for the parameters shown in the figure. The solid line represents the case where no cold photoelectrons are present, while the dashed line corresponds to the case where photoelectrons are present. As can be seen, the growth rates decrease monotonically with increasing θ for $\theta \leq 70^\circ$. However, beyond this point and in the range $70^\circ \leq \theta \leq 82^\circ$ the growth rates rise with θ , indicating a change in the nature of the instability. As was pointed out by Ma et al. (1987), the growth rates at $\theta \leq 70^\circ$ correspond to a kinetic instability due to the relative drift between the electrons and the lithium ions. This instability is similar to a current driven ion-acoustic instability in that the wave growth is due to Landau resonance with the electrons. Using the terminology introduced by Gary and Omidi (1987), we refer to this instability as the electron/ion-acoustic instability. The growth rates at $\theta \geq 70^\circ$, on the other hand correspond to a fluid type instability (for the temperatures considered here) due to the relative drift between the two ion species. This instability was referred to as the ion/ion-acoustic instability by Gary and Omidi (1987).

It is evident from Figure 2 that in the absence of photoelectrons, the ion/ion-acoustic instability has a maximum growth rate which is larger than that of the electron/ion-acoustic by an order of magnitude. Thus, in the absence of cold electrons the ion/ion-acoustic instability is probably the dominant one. On the other hand, the growth rates of the two instabilities are comparable when both electron species are present. This effect comes about by virtue of the fact that the electron/ion-acoustic waves grow due to Landau resonance with the electrons whose distribution function attains a larger slope in the presence of the cold electrons. Similarly the ion/ion-acoustic waves suffer a greater Landau damping due to the

increase in the slope of the electron distribution function. As was mentioned earlier these two instabilities are insensitive to the presence of a background magnetic field, and thus one would not expect to see any correlation between the electrostatic waves observed during the AMPTE release and the magnetic fluctuations in the solar wind.

The other set of instabilities which have been proposed to explain the electrostatic noise are the modified two stream instabilities [Papadopoulos et al., 1987]. These instabilities also arise due to either a drift between the electrons and the ions or two ion species. However, in either case the drift must be oblique to the direction of the magnetic field with the growth rates becoming maximum when the drift is perpendicular. To help better visualize the geometry of these instabilities we show in Figure 3 the coordinate system (ρ, η, ζ) in which the solar wind flow velocity (V_{SW}) is along the ρ -axis and the ambient magnetic field (B_0) is in the ζ direction. Also shown in Figure 3 is a typical wave vector \vec{k} which makes an angle ϕ with the ζ -axis and its projection on the (ρ, η) plane makes an angle θ with the ρ -axis. An important point to note is that unlike the ion-acoustic instabilities, the modified two stream instabilities are not axially symmetric with respect to the ρ -axis and thus both angles θ and ϕ play a role in the growth rates of the waves. Another important property of these instabilities is the fact that while in the low β regime they are well described by the electrostatic approximation, at larger values of β the electromagnetic effects become important and can lead to their stabilization (for more details on the modified two stream instabilities see, e.g. Gary et al., 1987). Since in the analysis of Papadopoulos et al. (1987) an approximate dispersion relation was utilized and also the value of β was taken to be zero, it is essential that their study be extended by using a full electromagnetic dispersion relation and allow for finite values of β .

The general electromagnetic form of the linear Vlasov dispersion equation for a

two-dimensional wave vector (\vec{k}) is given in Tokar and Gary (1985). Using this dispersion equation and the plasma parameters described earlier, growth rates have been calculated for a wide range of electron β (β_e) and angles θ and ϕ . The results of these computations for the same parameters shown in Figure 2 but without the cold electrons are shown in Figures 4-6. In Figure 4 the growth rates normalized to the proton angular gyrofrequency (Ω_i) and maximized over k are shown as a function of ϕ for a number of β_e values at $\theta = 0^\circ$. As was mentioned earlier, two types of instabilities are possible when the flow is across the magnetic field. One is due to the relative motion between the electrons and ions and is referred to as the electron/ion cross-field instability by Gary et al. (1987), while the other is due to the relative drift between the ions and is referred to as the ion/ion cross-field instability. The growth rates shown at $\phi \leq 88^\circ$ are due to the electron/ion cross-field instability while those at $\phi \geq 88^\circ$ are due to the ion/ion cross-field instability. As can be seen in Figure 4, the latter mode becomes stable as β_e is increased to about $\beta_e \sim 0.1$. It is also evident that as β_e increases the maximum growth rates decrease indicating that the electromagnetic effects become important and tend to stabilize both waves. It should, however, be mentioned that while the ion/ion mode becomes stable at $\theta = 0$ when β_e becomes large, it still remains unstable at other values of θ . To demonstrate this point, we show in Figure (5a) the maximum growth rates as a function of θ at $\phi = 88.5^\circ$ for four different values of β_e . The growth rates shown in this panel correspond to the ion/ion cross-field instability. As can be seen, when β_e is small (0.01) maximum growth rates peak at $\theta = 0^\circ$. However, as β_e increases the peak in γ_{\max} shifts to higher values of θ . Note that this effect is in contrast to that of the electron/ion mode whose growth rates are shown in panel (b) of Figure 5. As can be seen in this panel the growth rates drop monotonically with θ regardless of the value of β_e . Again it is evident in panel (a) of Figure 5 that the maximum growth rate of the ion/ion mode decreases with increasing β_e due

to the electromagnetic effects.

A point that should be mentioned in connection with Figure (5b) is that the growth rates at $\beta_e = 0.1$ are larger than those at $\beta_e = 0.5$ and in turn those growth rates are larger than the ones at $\beta_e = 0.01$. This effect is due to the fact that in Figure (5b) ϕ is kept fixed while β_e has changed. However, as can be seen in Figure 4, the value of ϕ at which γ_{\max} peaks varies with β_e . In short contrary to what might appear in panel (b) of Figure 5, the maximum growth rates of both of the instabilities decrease with increasing β_e .

Thus far the general behavior of the two cross-field instabilities have been investigated for various values of β_e . In order to determine the viability of these instabilities in generating the observed electrostatic noise, it is best to look at the real and the imaginary parts of the frequency as a function of K for a representative value of β_e . Using the plasma parameters given earlier ($n_e = 16\text{cm}^{-3}$, $T_e = 5 \times 10^5\text{ K}$) and a magnetic field strength of 23 (nT) (see Figure 1) we obtain the value of $\beta_e \sim 0.5$. Note that this value is probably a minimum in that the magnetic field strength used in its computation is the maximum observed value. Using this value of β_e , the real (ω_r) and the imaginary (γ) parts of the frequency have been calculated as a function of K for values of θ and ϕ at which maximum growth occurs. Note that the computations were carried out in a frame where the lithium ions are at rest which should correspond to that of the satellite. Panel (a) of Figure 6 shows ω_r (solid) and γ (dashed) for the ion/ion cross-field instability while panel (b) shows those of the electron/ion cross-field instability as a function of the wave number (K) times the proton gyroradius (ρ_i). Using the maximum magnetic field strength observed (23 nT) during the September 11 release, it is straightforward to compute the maximum growth rates of the two instabilities and their corresponding frequency and wavelength. As can be seen in Figure 6 the maximum growth rate of the ion/ion mode is $\gamma \simeq 4\Omega_i \simeq 9\text{ Hz}$, while that of the electron/ion mode is $\gamma \simeq 5\Omega_i \simeq 11.3\text{ Hz}$. A compar-

ison between these growth rates and those shown in Figure 2 clearly demonstrate that the growth rates of the ion-acoustic instabilities are more than an order of magnitude larger than those of the cross-field modes. It is also evident from Figure 6 that the maximum growth of the ion/ion cross-field instability occurs at a frequency $f \approx 17.5$ Hz while that of the electron/ion occurs at $f \approx 52$ Hz. Note, however, that these frequencies are too low to explain the observed spectrum. Finally both of the instabilities have maximum growth at a wave length of about $\lambda \approx 100$ km. These wavelengths also seem to be too large in view of the fact that they are comparable or larger than the entire size of the lithium cloud. Thus the results of linear theory indicate that the ion-acoustic instabilities are much more likely to have been responsible for the generation of the observed electrostatic noise.

2.2 Observations

In addition to linear theory, the measurements by the plasma wave instrument and the magnetometer can also be utilized to assess the plausibility of each set of instabilities having resulted in the generation of the electrostatic waves. This can be done by noting that while the ion-acoustic type instabilities are insensitive to the presence of an ambient magnetic field, the cross-field instabilities result in wave frequencies and growth rates which are sensitive to both the magnitude and the direction of the magnetic field. Specifically one would expect the wave frequencies of the cross-field instabilities to increase with the ambient magnetic field strength, and also the wave power to rise (fall) as the magnetic field direction becomes more (less) oblique to the solar wind flow direction. Note also that one would not expect the cross-field instabilities to be operative when the solar wind flow is parallel or quasi-parallel to the magnetic field. The September 11th release is particularly suitable for conducting this test in that both the magnitude and the direction of the magnetic field changed considerably during the period when the electrostatic waves

were observed (Lühr et al., 1986). For example, it is evident in the third panel of Figure 1 that the magnetic field varies from $B \approx 8\text{nT}$ at 07:25:30 UT to $B \approx 23\text{nT}$ at 07:25:35 UT and then drops back to $B \approx 11\text{nT}$ at 07:25:38 UT. Similarly, assuming the solar wind flow to be along the Sun-Earth line in the GSE coordinate system (i.e. $\phi_B = 360^\circ$ and $\theta_B = 0^\circ$), it is clear from the top two panels in Figure 1 that the magnetic field direction changes considerably with respect to the flow velocity.

The eight panels in Figure 7 show the electric field spectrum densities during the period 07:25:30.2 - 07:25:38 UT. The beginning of this period corresponds roughly to the onset of the electrostatic waves with the power reaching its maximum at about 07:25:35. Beyond this time, the wave amplitudes decrease approaching the background level at around 07:25:40 UT. One striking feature of the power spectrums shown in Figure 7 is the fact that while the shape of the spectrums change with time, the maximum power remains at a relatively fixed frequency of $f \sim 150\text{ Hz}$. This feature argues against the cross-field instabilities being responsible for the amplification of the waves in two ways. First, the frequencies at peak power are much larger than the frequencies ($f \lesssim 50\text{ Hz}$ assuming $B = 23\text{nT}$) at which cross-field instabilities have maximum growth rates. Second, since the magnetic field strength varies considerably during the time interval considered in Figure 7, one would expect the frequencies at peak power to vary accordingly. This effect, however, is not reflected in the power spectrums shown in Figure 7. In regards to the direction of the magnetic field it is evident from the top two panels of Figure 1 that both ϕ_B (azimuthal angle) and θ_B (latitudinal angle) fluctuate by as much as 30° on relatively short time scales. These fluctuations however, do not seem to affect the intensity of the waves. In addition, while the magnetic field may at times be oblique to the flow direction, it is far from being perpendicular to it. Again suggesting that the prevailing conditions in the plasma are not conducive to the generation of waves via the cross-field instabilities.

In short both theoretical investigations as well as observational evidence indicate that the electrostatic waves observed during the AMPTE solar wind releases were generated by the ion-acoustic type instabilities.

3. NONLINEAR ANALYSIS

3.1 General Remarks

Thus far we have considered two sets of instabilities with the main distinction between the two being that one set requires the presence of a background magnetic field while the other can exist in an unmagnetized plasma. Having shown that the ion-acoustic type instabilities are the dominant modes, the remainder of this paper will be devoted to the nonlinear evolution of the waves. A point to note is that while the electron/ion-acoustic and the ion/ion-acoustic instabilities result in plasma waves with similar dispersive properties (i.e. acoustic like), it is nonetheless essential that these two instabilities be distinguished when considering their nonlinear evolution. This is because the source of free energy and therefore, the saturation mechanism of each instability is different. Specifically, the electron/ion-acoustic waves grow due to Landau resonance with the electrons and therefore, are expected to saturate via quasi-linear diffusion of the electrons and formation of a plateau in their distribution function. Because the time scales associated with this process are small as compared to ion time scales, one would not expect the electron/ion-acoustic instability to affect the ions in an appreciable way. On the other hand the ion/ion-acoustic waves grow due to interaction between the two ion species and thus their saturation mechanism must involve ions. This can also be seen by noting that any heating of the electrons by the waves will tend to increase the ratio of T_e/T_p which enhances the growth rates (see e.g. Gary and Omidi, 1987). In other words, electron heating does not have a stabilizing effect on the ion/ion-acoustic waves.

As can be seen in Figure 2 when both the cold photoelectrons as well as the hot solar wind electrons are present the maximum growth rates of the electron/ion-acoustic and the ion/ion-acoustic waves are comparable. Thus, it is conceivable that

both modes may grow with the electron/ion waves heating the cold electrons and the ion/ion waves interacting mainly with the two ion populations. On the other hand, when no cold electrons are present the ion/ion mode becomes dominant. Although the effect of waves on the electrons is interesting, our main goal is to see how the newly born ions are affected by the waves, that is to say, how the observed waves could have resulted in coupling between the solar wind protons and the lithium or barium ions. Thus we need only be concerned with the ion/ion mode and investigate its nonlinear evolution. To this end, one-dimensional electrostatic particle simulations have been performed, the results of which are presented here. These results correspond to two classes of simulations; one in which the electrons and the ions are treated as particles with the disadvantage of an unrealistic mass ratio between the electrons and the ions. The other set of results correspond to a simulation code in which the electrons are approximated by a Boltzman fluid. This code has the advantage that the electron to ion mass ratio is realistic and therefore the observed plasma parameters can be used in the simulations.

3.2 Full Particle Simulations

The full particle simulation model consists of a one-dimensional periodic box in the direction of the \vec{K} vector (e.g. the x-axis in Figure 3 when $\Phi = 90^\circ$). Note that the \vec{K} vector can be directed in any desired direction by assigning the flow velocity of each plasma species to be equal to its original flow velocity projected along the desired direction. Thus for example, in order to simulate the waves propagating at an angle θ with respect to the solar wind flow direction (\vec{V}_{SW}) it is sufficient to assign the solar wind velocity to be $V_{SW} \cos \theta$. The simulation results presented in this paper all correspond to a case where no photoelectrons are present, and thus, the ion/ion mode has growth rates that are larger than those of the electron/ion mode by an order of magnitude. This is desirable since our primary interest is in the ion/ion

mode. Also the fact that the ion/ion mode has larger growth rates makes the use of a one-dimensional model appropriate in view of the fact that even in a two-dimensional model the electron/ion modes would not have had a chance to grow. This point will be substantiated later when it is shown that the ions become disrupted on time scales shorter than the growth time of the electron/ion mode. The size of the simulation box is 32 electron Debye lengths (λ_e), and it consists of 64 cells. The simulation frame is taken to be the same as that in the linear theory and thus, initially the lithium ions form a non-drifting Maxwellian while the solar wind protons consist of a Maxwellian drifting with velocity $V_{sw}\cos\theta$. Similarly the electrons have a drift speed such that the net current is zero.

As mentioned earlier, one of the difficulties associated with a full particle code is the fact that the simulation must account for the electron dynamics. Therefore, the time steps in the simulations must be small enough such that the electron dynamics are resolved. On the other hand, since the ion/ion mode involves the motion of the ions which takes place on a much longer time scale it is not feasible to use a realistic mass ratio between the electrons and the ions. Thus, it is necessary to adjust the ratio of the masses such that both the electron and the ion dynamics can be simultaneously resolved. For this reason we use $m_{Li} = 6m_p = 600m_e$ where Li, p, and e stand for lithium, proton and electron respectively and m is the mass.

Although the use of unrealistic mass ratios does not usually change the physical nature of the problem, it does make it impossible to use the exact plasma parameters as those in a realistic plasma. The results of the full particle simulation presented here correspond to the following plasma parameters. The proton flow velocity $V_{sw} = 0.71v_e$, its thermal velocity $v_p = 0.01v_e$ where v_e is the electron thermal speed. The lithium thermal velocity $v_{Li} = 0.26 \times 10^{-2}v_e$, the angle of propagation $\theta = 85^\circ$, and the lithium density $N_{Li} = N_p$. In these simulations the electrons are represented by

32,000 particles while the protons and the lithium ions are each represented by 16,000 particles. The time step $\Delta t = 0.2\omega_{pe}^{-1}$ where ω_{pe} is the electron plasma frequency. Finally, it should be mentioned that the simulations are carried out as an initial value problem where the system is allowed to evolve in time without a constant refurbishing of new particles.

The four panels in Figure 8 show the energy history of the electrostatic waves, electrons, protons, and the lithium ions from top to bottom respectively. These energies are normalized to the total initial energy in the system. As can be seen in the top panel, initially the wave energy increases with time till it eventually saturates at about $t \approx 560\omega_{pe}^{-1}$. Thus during this period the ion/ion waves are growing with time. Beyond $t = 560\omega_{pe}^{-1}$ the wave energy begins to decrease due to damping by wave-particle interactions. The damping of the waves lasts until about $t \approx 700\omega_{pe}^{-1}$, when the level of fluctuations becomes more steady with time. The second panel in Figure 8 shows the energy history of the electrons which closely mimics that of the waves. This behavior is in contrast to the energy history of the protons and the lithium ions. As can be seen, the protons which are the source of free energy for wave amplification, lose energy with time until $t \approx 560\omega_{pe}^{-1}$. Beyond this point, their energy remains relatively constant with time. The lithium ions gain energy throughout the run, although the rate of increase becomes quite small after $t \approx 675\omega_{pe}^{-1}$. The behavior of the protons and the lithium ions substantiate the expectation that the ion/ion mode can greatly affect the ions. One of the interesting aspects of Figure 8 is the fact that the energy history of the electrons and the waves are very similar. This suggests that the observed changes in the energy of the electrons must be for the most part due to coherent motion in the electric field of the waves, rather than random motions which cause an increase in their temperature. This point will be further substantiated later.

To better understand the role of the wave-particle interactions on ion dynamics

the phase space density plots (V_x vs x) of the protons and the lithium ions are shown in Figures 9 and 10 at three separate times during the simulations. In these figures, the velocity of each species is normalized to its thermal speed. As can be seen in panel (a) of Figure 9, initially the protons form a beam with a drift speed $v_d = 0.71 \cos(85^\circ) v_e \approx 6.2 v_p$. At later times when the waves have grown, they begin to interact with the protons (panel b) leading to their eventual trapping (panel c). Note in panel (b) that six oscillations are present, which agrees with the results of linear theory indicating that modes 5 and 6 are the most unstable ones. From the number of trapping vortices in panel (c), however, it is clear that mode number 5 has become dominant at later times. Note also that the center of the trapping vortices lies around $V_x \approx 2 v_p$ which is reasonable in view of the fact that the phase velocity of the unstable waves is $V_\phi \approx 1.7 v_p$. The phase space density plots of the lithium ions presented in Figure 10 show that initially, these ions have a zero drift velocity. At later times during the simulation, the lithium ions begin to interact with the waves resulting in the oscillations shown in panel (b). Note again that six oscillations can be seen during this relatively early stage of the simulation. Panel (c) of Figure (10) shows the lithium ions becoming trapped, indicating that the nonlinear saturation mechanism of the ion/ion mode is in this case trapping of both of the ion species. This behavior may at first seem somewhat surprising in that the trapping frequency $\omega_T \equiv \left(\frac{qKE}{m}\right)^{1/2}$ (where E is the electric field amplitude, q and m are the charge and mass of the particle) of each species is proportional to the inverse square root of its mass. Thus, ordinarily one would expect the protons to get trapped and saturate the instability before the lithium ions have had a chance to get trapped. The fact that in this case both species suffered trapping can be explained by noting that the phase velocity of the waves $V_\phi \approx 1.7 v_p$, falls closer to the lithium ion distribution as compared to that of the protons whose beam speed is $V_d = 6.2 v_p$. Thus, in order for the protons to get trapped they must first get decelerated by a substan-

tial amount, and a large electric field must be set up. This, however, requires a longer time which implies a smaller effective trapping frequency for the protons. In other words due to the large flow velocity of the protons relative to the phase speed of the waves, their effective trapping frequency becomes comparable to that of the lithium ions whose velocity distribution function lies closer to the phase velocity of the waves.

In order to understand in more detail the effect of wave-particle interactions on the electrons, their velocity distribution functions at $t = 0$ and $600\omega_{pe}^{-1}$ are shown in Panels (a) and (b) of Figure 11. As can be seen the initial Maxwellian distribution function of the electrons remains unchanged, although the densities (counts) do change with time. Panel (c) of Figure 11 shows the density profile of the electrons at $t = 600\omega_{pe}^{-1}$. Note that the fluctuations are as much as 50%. The fact that the temperature and the distribution function of the electrons remain unchanged throughout the run, further substantiates the suggestion made earlier that the electrons move in a coherent manner in the potential field of the waves. Therefore, as the waves grow the energy of the electrons also increases, and as waves get damped their energy decreases. This behavior of the electrons suggests that they may be approximated as a charge neutralizing fluid when considering the ion/ion mode. Such an approximation is desirable, because in the simulations one would not have to be concerned with the electron dynamics, and therefore realistic mass ratios between the electrons and the ions can be used.

3.3 Simulations with Boltzman electrons

To approximate the electrons as a charge neutralizing fluid, use can be made of the Boltzman's relation

$$n_e(x) = n_0 \exp(e\Phi(x)/T_e) \quad (1)$$

which gives the electron density at any position $n_e(x)$ as a function of the electrostatic potential $\Phi(x)$ at that position, the background (or unperturbed) density n_0 , and the electron temperature T_e (where the Boltzman constant k is absorbed in T_e). The use of equation (1) is expected to be quite satisfactory when the density fluctuations are small relative to n_0 , and therefore can be thought of as perturbations. On the other hand once the wave amplitudes become sufficiently large, such that the density fluctuations are a large percentage of n_0 , it is not obvious if and why relation (1) should hold. In fact if the ion density (n_i) fluctuations become large one might think that a better approximation for the electrons may be to replace n_0 in equation (1) with $n_i(x)$. To see which one of these methods better approximates the actual density of the electrons, the expressions $n_0 \exp(e\Phi/T_e)$ and $n_i \exp(e\Phi/T_e)$ have been computed at $t = 600\omega_{pe}^{-1}$ and shown in panels (d) and (e) of Figure 11 respectively. Note that in our case, $n_i(x)$ is the sum of the proton and lithium densities at position x . A comparison of panels (d) and (e) with (c) clearly indicates that even in the presence of large amplitude waves, the use of n_0 provides a better approximation to the density of the electrons. Note, however, that even in this case notable differences between Panels (c) and (d) exist, suggesting that the Boltzman approximation is not a perfect one.

In order to evaluate the usefulness of the Boltzman approximation in studying the nonlinear evolution of the ion/ion mode, a test simulation run was performed. This run was similar in all aspects (i.e. plasma parameters, mass ratios, etc.) to the full particle run except for the fact that the electrons were approximated by equation (1). The full nonlinear Poisson's equation was solved for using the Newton iteration method [Hockney and Eastwood, 1981]. The phase space density plots of the protons and the lithium ions at $t = 600\omega_{pe}^{-1}$ from the test run are shown in panels (a) and (b) of Figure 12 respectively. A comparison between this figure and panels (c) in Figures 9 and 10 shows that aside from minor details, the results are

identical. This clearly demonstrates the validity and the usefulness of the Boltzman approximation in describing the nonlinear physics of the ion/ion instability.

As mentioned earlier, the fluid description of the electrons allows one to use plasma parameters that could correspond to the observation. In the remainder of this section the results of a simulation run with realistic plasma parameters are presented. The length of the simulation box (L) is 64 proton Debye lengths (λ_p) and consists of 64 cells. Each of the ion species are represented by 16,000 particles and the time step $\Delta t = 0.2\omega_{pi}^{-1}$ where ω_{pi} is the proton gyrofrequency. Figure 13 shows the growth rates (γ) of the ion/ion instability as a function of the mode number ($\frac{LK}{2\pi}$) for the parameters shown in the figure. These parameters are similar to those used by Gurnett et al. (1986a,b) and are used in the simulation run. As can be seen, the growth rates peak at mode number 4 and thus one would expect this mode to be dominant in the simulation. Note, however, that the growth rates of modes 3 and 5 are also appreciable and thus these modes may also show up in the simulations. Panel (a) of Figure 14 shows the electric field of the waves as a function of x at $t = 60\omega_{pi}^{-1}$ during the simulation. It is evident from this panel that the wave amplitude varies with x or in other words is being modulated. To determine which modes have been excited, a Fourier analysis of the electric field squared has been performed and is shown in panel (b) of Figure 14. As can be seen the peak in the spectrum corresponds to mode 4 with modes 3 and 5 having the second and the third largest power respectively. This result is in good agreement with the linear theory. Note that although the growth rates of modes 3 and 5 are comparable, one would still expect mode 3 to have larger power due to the fact that the initial noise level in the system drops with increasing K .

Figure 15 shows the phase space density plot of the protons at three separate times. It is evident in panel (a) of Figure 15 that initially the protons have a drift speed $V_d \approx 2.2v_p$ which is smaller than the beam speed of the protons in the full

particle simulation. The phase velocity of the unstable waves $V_\phi \approx 0.46v_p$ which falls within the distribution function of the protons. Thus, one would expect the trapping of the protons to take place on a faster time scale as compared to the full particle simulation. It can be seen in panel (b) of Figure 15, that four trapping vortices have been formed as expected from the Fourier analysis of the waves. Note, however, that the two vortices on the right hand side of the box are more pronounced due to the fact that the electric field of the wave is larger on that side of the box. Panel (c) of Figure 15 shows the protons at later time when the vortices have begun to collapse leading to the scattering of the protons in phase space. Note that the vortex on the right hand side corresponds to the vortex between $32 \leq x \leq 48 \lambda_p$ shown in panel (b). Similarly the remnants of the vortex between $48 \leq x \leq 64 \lambda_p$ in panel (b) can be seen at $0 \leq x \leq 16 \lambda_p$ in panel (c). The observed speed of the vortices is near the phase velocity of the waves as one would expect.

The phase space density plots of the lithium ions are shown in Figure 16 for the same times as those in the previous figure. Initially these ions form a cold non-drifting Maxwellian (panel a). As the waves grow, the lithium ions are accelerated by their electric field, leading to the observed fluctuations in panels (b,c). Note however, that these ions have not become trapped in the potential well of the waves in contrast to the protons (see panel (b) of Fig. 15). As mentioned earlier this behavior is expected since the trapping time for the lithium ions is longer than that of the protons. The fact that the phase velocity of the growing waves falls within the distribution function of the protons results in their rapid trapping, and saturation of the instability before the lithium ions get trapped. Despite this, however it is evident that some of the lithium ions are accelerated to relatively large velocities by the electric field of the waves.

These results clearly indicate that the saturation mechanism of the ion/ion mode remains to be ion trapping when realistic plasma parameters are used. Nonetheless,

differences between the two cases also exist, in that the effect of the waves on the heavier ions is not as pronounced when the observed plasma parameters are used. Simulations with barium ions have shown similar results in that the instability saturates via proton trapping and the much heavier barium ions are not strongly scattered in phase space. A point that should also be noted is that the observed heating and acceleration of the ions is along the \vec{k} vector of the ion/ion wave which is oblique to the solar wind flow velocity. Implications of these results in regards to the role of the ion/ion mode in providing coupling between flowing plasmas and the new born ions is discussed in the next section.

4. SUMMARY AND DISCUSSION

4.1 Summary

In this paper the nature and the nonlinear evolution of the electrostatic waves observed during the AMPTE solar wind releases was investigated. By using the full electromagnetic dispersion relation the properties of the electron/ion and the ion/ion cross-field instabilities were studied and their growth rates were calculated for the plasma parameters representative of those during the AMPTE releases. It was shown that these growth rates are an order of magnitude or more smaller than those of the electron/ion-acoustic and the ion/ion-acoustic instabilities. The linear analysis of the cross-field instabilities also show that the wavelength of the maximum growing wave is about 100 km which is comparable to the size of the cloud and therefore not likely to occur. Similarly the frequencies of the cross-field modes were shown to be much smaller than the observed frequencies. By using the magnitude and the direction of the ambient magnetic field measured during the September 11 lithium release, and also the wave electric field spectrums, it was shown that neither the frequency nor the intensity of the observed waves correlate in any clear manner with the changes in the magnetic field. Since one would expect such a correlation to exist had the waves been generated by the cross-field instabilities, it was clear that the observations do not support the suggestion by Papadopoulos et al. (1987) that the electrostatic waves were generated by the cross-field instabilities. In view of both theoretical and observational evidence it was concluded that the electrostatic waves associated with the AMPTE solar wind releases were generated by the ion-acoustic type instabilities.

Because among the two ion/acoustic type instabilities the ion/ion mode can lead to heating and acceleration of the ions, the nonlinear evolution of this instability was investigated via numerical simulations. By using a full particle electrostatic

code it was illustrated that the saturation mechanism of the ion/ion-acoustic instability is ion trapping, while the electrons behave as a charge neutralizing fluid. Because of this characteristic of the ion/ion instability, it was possible to conduct a simulation study in which the electrons were treated as a Boltzman fluid, thus allowing for realistic plasma parameters to be used. The results of this simulation study confirmed the conclusions reached by the full particle code that the saturation mechanism of the ion/ion mode is ion trapping and that this process could take place using realistic prarmeters. In spite of these similarities, however, differences between the two simulation studies also exist. A major difference being that unlike the full particle simulations in which both the protons and the lithium ions became trapped, in the Boltzman electron simulations only the protons became trapped. This contrast was attributed to the fact that in the former case the proton drift speed was much larger than the wave phase speed indicating that the protons would first have to be decelerated, and then trapped; thereby increasing their effective trapping period. This increase in the trapping period of the protons then made it possible for both of the ion species to interact strongly with the waves. On the other hand, during the fluid electron simulations the phase velocity of the unstable waves fell within the proton distribution function, resulting in their more rapid trapping.

4.2 Discussion

The results presented here clearly show that the ion/ion-acoustic instability can to some degree result in transfer of energy and momentum from ions of a flowing plasma to the newly created ions. A question that arises then is how effective this mechanism can be as compared to the other modes that may also be generated due to the collective plasma processes. Obviously ,the answer may to some extent depend on the situation under investigation. For example it was suggested by Winske et al. (1984, 1985) that during the AMPTE releases in the solar wind low frequency elec-

tromagnetic waves could be generated by the ion-beam instabilities. However, because of their long wave length relative to the cloud size these waves could not have been generated in the initial stages of the cloud expansion, and thus, the ion/ion-acoustic mode would play a dominant role. On the other hand at times or places (e.g. comets) where the electromagnetic waves can grow to large amplitudes they become very effective in transferring energy and momentum between the ion species (see e.g. Winske et al., 1984 and Omid and Winske, 1987). Whether in such situations the ion/ion-acoustic instability can play a dominating role on ion dynamics is a subject of further investigation. However, the results presented in Figure 16 do not suggest so. For example, using the plasma parameters of these simulations it can be shown that the lithium thermal speed corresponds to $v_L = 1.84$ km/s. From panel (c) of Figure 16 it is evident that some lithium ions have been accelerated to velocities as high as 40 km/s while the majority of the ions have velocities around and below 20 km/s. These speeds, however, are less than 10% of the solar wind flow velocity and therefore not considerable in terms of what is required to assimilate the ions into the solar wind. This is in contrast to the pick-up by the electromagnetic waves which can result in average flow velocities for picked-up ions that are 50% of the solar wind speed (e.g. Omid and Winske, 1987). Nonetheless the ion/ion-acoustic waves may also play an important role in the pick-up process. To further investigate this process it is best to use simulation models with non-periodic boundary conditions so that a constant refurbishing of the solar wind protons can take place. The advantage of such a model which is more realistic is that the instability may not become saturated as early as it does in a periodic system. Observations of the electrostatic waves during the AMPTE releases in the solar wind as well as at comet Giacobini-Zinner (Sarf et al., 1986) are good encouragements for conducting such studies in the future.

ACKNOWLEDGEMENTS

The authors would like to thank H. Lühr for the use of his magnetometer data, and S.P. Gary for the use of his electromagnetic dispersion code. One of the authors (N.O.) would also like to thank K.B. Quest for providing him with the original version of the electrostatic code. The research at UCLA was supported by NASA (STTP) NAGW-78, Air Force Grant F-19628-85-K-0027, and the National Science Foundation Grant ATM85-13215. The work at Los Alamos was supported by the DOE Office of Basic Energy Sciences, Geosciences and by the Institute of Geophysics and Planetary Physics at Los Alamos National Laboratory. The research at the University of Iowa was supported by the Office of Naval Research through contract N00014-82-K-0183 and by NASA Headquarters through grant NGL-16-001-043.

REFERENCES

- Akimoto, K. and N. Omidi, The generation of broadband electrostatic noise by an ion beam in the magnetotail, Geophys. Res. Lett., 13, 97, 1986.
- Brinca, A.L., A.A. Moreira, F.M. Serra, G. Haerendel, and G. Paschmann, Complementary analysis and interpretation of the shocklike electrostatic noise observed during the AMPTE solar wind lithium release, J. Geophys. Res., 91, 10167, 1986.
- Gary, S.P., and N. Omidi, The ion/ion-acoustic instability, J. Plasma Phys., 37, 45, 1987.
- Gary, S.P., R.L. Tokar and D. Winske, Ion/ion and electron/ion cross-field instabilities near the lower hybrid frequency, J. Geophys. Res., submitted, 1987.
- Gurnett, D.A., R.R. Anderson, B. Häusler, G. Haerendel, O.H. Bauer, R.A. Treumann, H.C. Koons, and R.H. Holzworth, Plasma waves associated with the AMPTE artificial comet, Geophys. Res. Lett., 11, 851, 1985.
- Gurnett, D.A., T.Z. Ma, R.R. Anderson, O.H. Bauer, G. Haerendel, B. Häusler, G. Paschman, R.A. Treumann, H.C. Koons, R. Holzworth, and H. Lühr, Analysis and interpretation of the shocklike electrostatic noise observed during the AMPTE solar wind lithium releases, J. Geophys. Res., 91, 1301, 1986a.
- Gurnett, D.A., T.Z. Ma, R.R. Anderson, G. Haerendel, G. Paschmann, O.H. Bauer, R.A. Treumann and H.C. Koons, R.H. Holzworth, and H. Lühr, Waves and electrical fields associated with the first AMPTE artificial comet, J. Geophys. Res., 91, 10031, 1986b.
- Häusler, B., L.J. Woolliscroft, R.R. Anderson, D.A. Gurnett, R. Holzworth, H.C. Koons, O.H. Bauer, G. Haerendel, R.A. Treumann, P.J. Christiansen, A.G. Darbyshire, M.P. Gough, S.R. Jones, A.J. Norris, H. Lühr, and N. Klöcker, Plasma waves observed by the IRM and UKS spacecraft during the AMPTE solar wind lithium releases: overview, J. Geophys. Res., 91, 1283, 1986.

- Hockney, R.W. and J.W. Eastwood, Computer Simulation Using Particles, McGraw-Hill, New York, 1981.
- Lühr, H., D.J. Southwood, N. Klöcker, M. Acuna, B. Häusler, M.W. Dunlop, W.A.C. Mier-Jedrzejowicz, R.P. Rijnbeck, and M. Six, In situ magnetic field measurements during the AMPTE solar wind Li^+ releases, J. Geophys. Res., **91**, 1261, 1986.
- Ma, T.Z., D.A. Gurnett and N. Omidi, An analysis of the shock-like electrostatic noise observed during AMPTE solar wind ion releases, J. Geophys. Res., **92**, 2555, 1987.
- Omidi, N., T.Z. Ma, K. Quest, M. Ashour-Abdalla, D. Gurnett and R. Sydora, Simulation and non-linear stage of the electrostatic waves observed during the AMPTE lithium release in the solar wind, Adv. in Space Res., in press, 1987.
- Omidi, N., and D. Winske, A kinetic study of solar wind mass loading and cometary bow shock, J. Geophys. Res., in press, 1987.
- Papadopoulos, K., J.D. Huba and A.Y.T. Lui, Collisionless coupling in the AMPTE artificial comet, J. Geophys. Res., **92**, 47, 1987.
- Scarf, F.J., F.V. Coroniti, C.F. Kennel, D.A. Gurnett, W.H. Ip and E.J. Smith, Initial report on plasma wave observations at comet Giacobini-Zinner, Science, **232**, 1986.
- Tokar, R.L. and S.P. Gary, The Whistler mode in a Vlasov plasma, Phys. Fluids, **28**, 1063, 1985.
- Winske, D., C.S. Wu, Y.Y. Li, and G.C. Zhou, Collective capture of released lithium ions in the solar wind, J. Geophys. Res., **89**, 7327, 1984.
- Winske, D., C.S. Wu, Y.Y. Li, Z.Z. Ma, Y.S.Y. Guo, Coupling of newborn ions to the solar wind by electromagnetic instabilities and their interaction with the bow shock, J. Geophys. Res., **90**, 2713, 1985.

FIGURE CAPTIONS

- Figure 1 One minute measurements by the magnetometer and the plasma wave instrument during the September 11 lithium release in the solar wind are shown. The top three panels show the direction (azimuthal and latitudinal angles in GSE coordinates) and the magnitude of the magnetic field while the bottom panel shows the electric field spectogram. The onset of the intense electrostatic waves is at about 07:25:30 UT.
- Figure 2 The growth rates of the ion/ion-acoustic and the electron/ion-acoustic instabilities maximized over the wave number are shown as a function of the angle (θ) between the \vec{k} vector and the solar wind velocity. The solid line represents the growth rates in the absence of cold electrons, while the broken line corresponds to the case where photoelectrons are present. For the plasma parameters shown the ion/ion-acoustic instability occurs at $\theta \geq 70^\circ$.
- Figure 3 The relative orientations of the solar wind velocity (V_{SW}), the ambient magnetic field (B_0) and the \vec{k} vector of the waves in the (ρ, η, ζ) coordinate system are shown.
- Figure 4 The growth rates of the ion/ion cross-field instability ($\Phi \approx 88^\circ$) and the electron/ion cross-field instability maximized over \vec{k} are shown as a function of Φ at four values of electron β_e . In this figure $\theta = 0^\circ$ and thus k lies in the (ρ, ζ) plane. Note that as β_e increases the growth rates become smaller due to electromagnetic effects. Ω_i is the proton gyrofrequency.
- Figure 5 The growth rates of the ion/ion cross-field instability (panel a) and the electron/ion cross-field instability (panel b) maximized over k are plotted as a function of θ for a number of electron β_e . Note that the growth

rates of the ion/ion mode peak at larger values of θ as β_e increases while the maximum growth of the electron/ion mode occurs at $\theta = 0^\circ$ for all values of β_e .

Figure 6 The real (solid) and the imaginary (broken) parts of the frequency corresponding to the ion/ion cross-field (panel a) and the electron/ion cross-field (panel b) instabilities are plotted as a function of K for $\beta_e = 0.5$ and values of θ and ϕ at which maximum growth occurs. ρ_i is the proton gyroradius.

Figure 7 In this figure eight electric field power spectrums covering the period 07:25:30.2 - 07:25:38 are shown. Note that despite the large changes in the magnetic field strength during this period the frequency at peak power remains relatively fixed ($f \gtrsim 100$ Hz), and at values much larger than those predicted by the cross-field instabilities.

Figure 8 The energy history of the electrostatic waves, electrons, protons, and the lithium ions are shown from top to bottom panels respectively. Note that the energy history of the electrons is similar to that of the waves.

Figure 9 The phase space density plots of the protons are shown at three different times during the simulations. Initially (panel a) the protons form a beam. At later times they get decelerated (b) and trapped (c) in the electric potential of the waves which eventually leads to their scattering in phase space.

Figure 10 The phase space density plots of the lithium ions are shown at three different times during the simulations. As can be seen the lithium ions also interact strongly with the excited waves leading to their acceleration and eventual scattering in phase space.

Figure 11 The velocity distribution function of the electrons at $t = 0$ and $600\omega_{pe}^{-1}$ are shown. As can be seen the electrons do not experience any heating

due to the wave-particle interactions. Panels (c), (d), and (e) show the electron density, $n_0 \exp(e\Phi/T_e)$, and $n_i \exp(e\Phi/T_e)$ as a function of x at $t = 600\omega_{pe}^{-1}$. Note that the electron density profile is best approximated by $n_0 \exp(e\Phi/T_e)$.

Figure 12 The phase space density plots of the protons and the lithium ions obtained from a simulation code with Boltzman electrons are shown in panels (a) and (b) respectively. A comparison between these panels and panel (c) in Figures 9 and 10 clearly demonstrates the validity of the Boltzman approximation for the electrons.

Figure 13 The growth rates γ of the ion/ion-acoustic mode for the plasma parameters shown in the figure are plotted as a function of mode number ($\frac{KL}{2\pi}$). Note that the growth rates peak at mode number 4.

Figure 14 The electric field profile and its power spectrum at $t = 60\omega_{pi}^{-1}$ during the simulation are shown in panels (a) and (b) respectively. Note that in agreement with linear theory the largest power occurs at mode number 4.

Figure 15 The phase space density plots of the protons are shown at three different times during the simulations. As can be seen, similar to the full particle case the protons become trapped and later scatter in phase space due to interaction with the excited waves.

Figure 16 The phase space density plots of the lithium ions are shown at three different times during the simulations. Note that while these ions undergo some interaction with the waves they do not become trapped in the potential field of the waves.

AMPTE-IRM Day 255 Sept 11, 1984

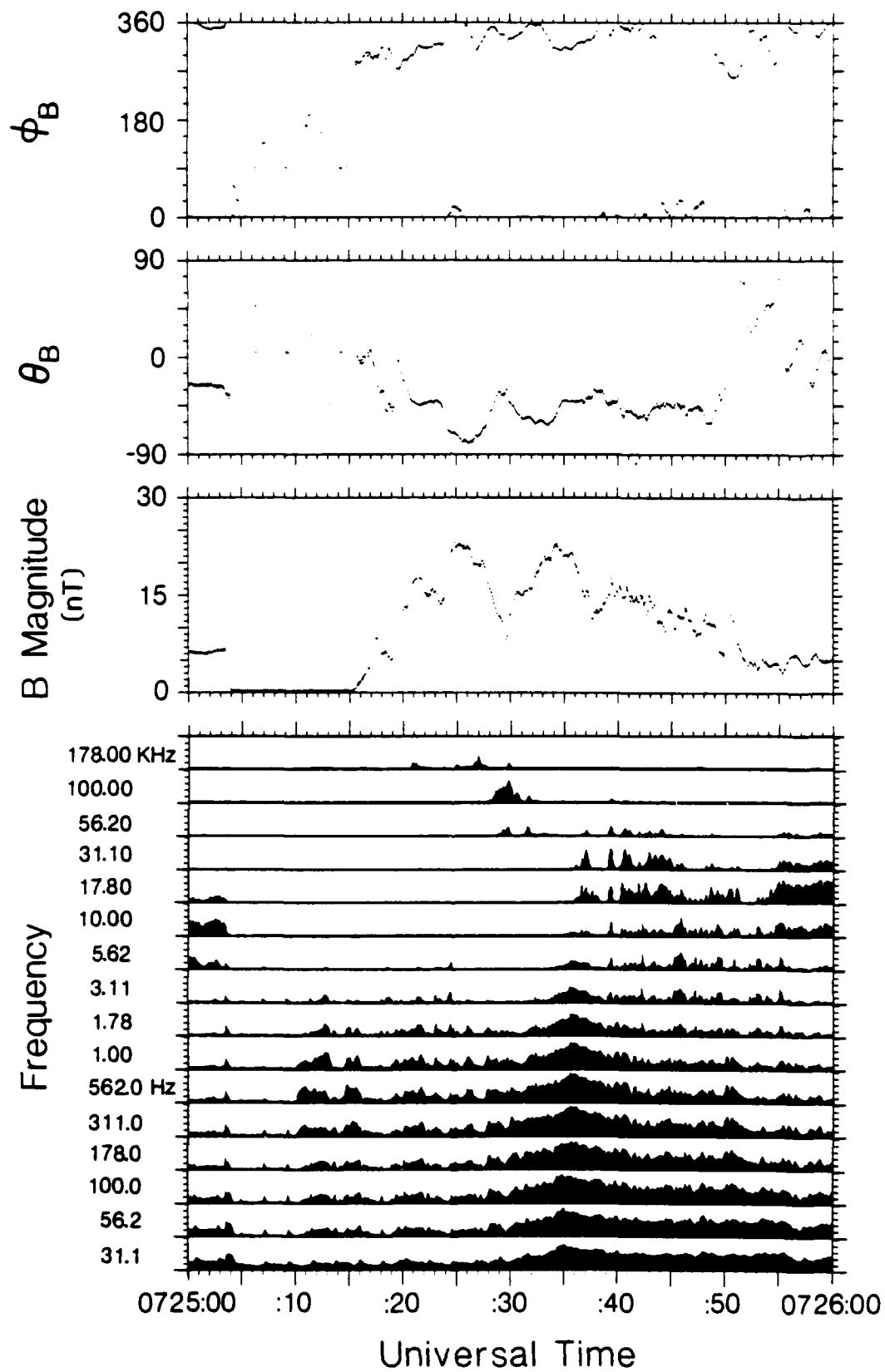


Figure 1

A-G86-65

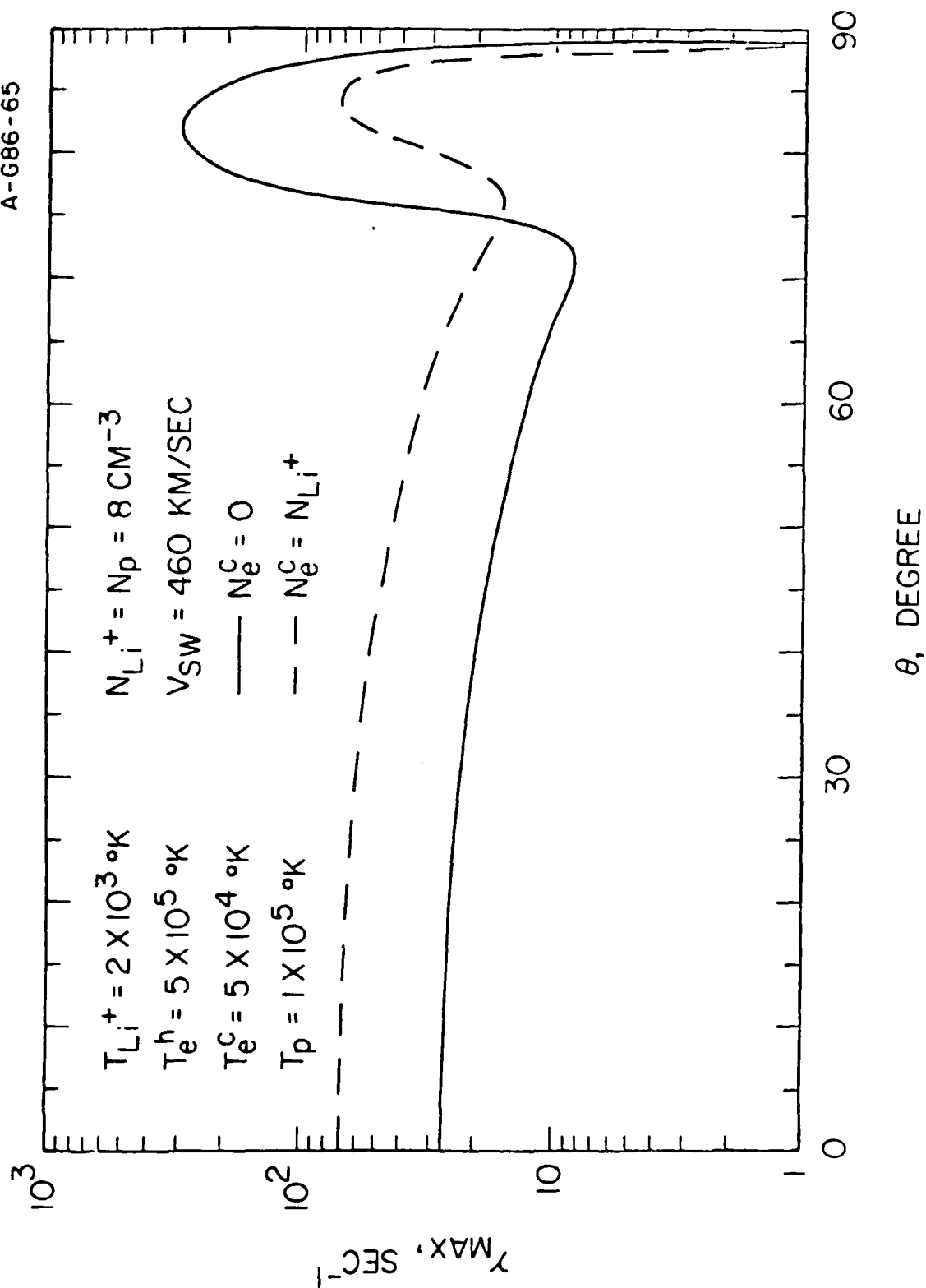


Figure 2

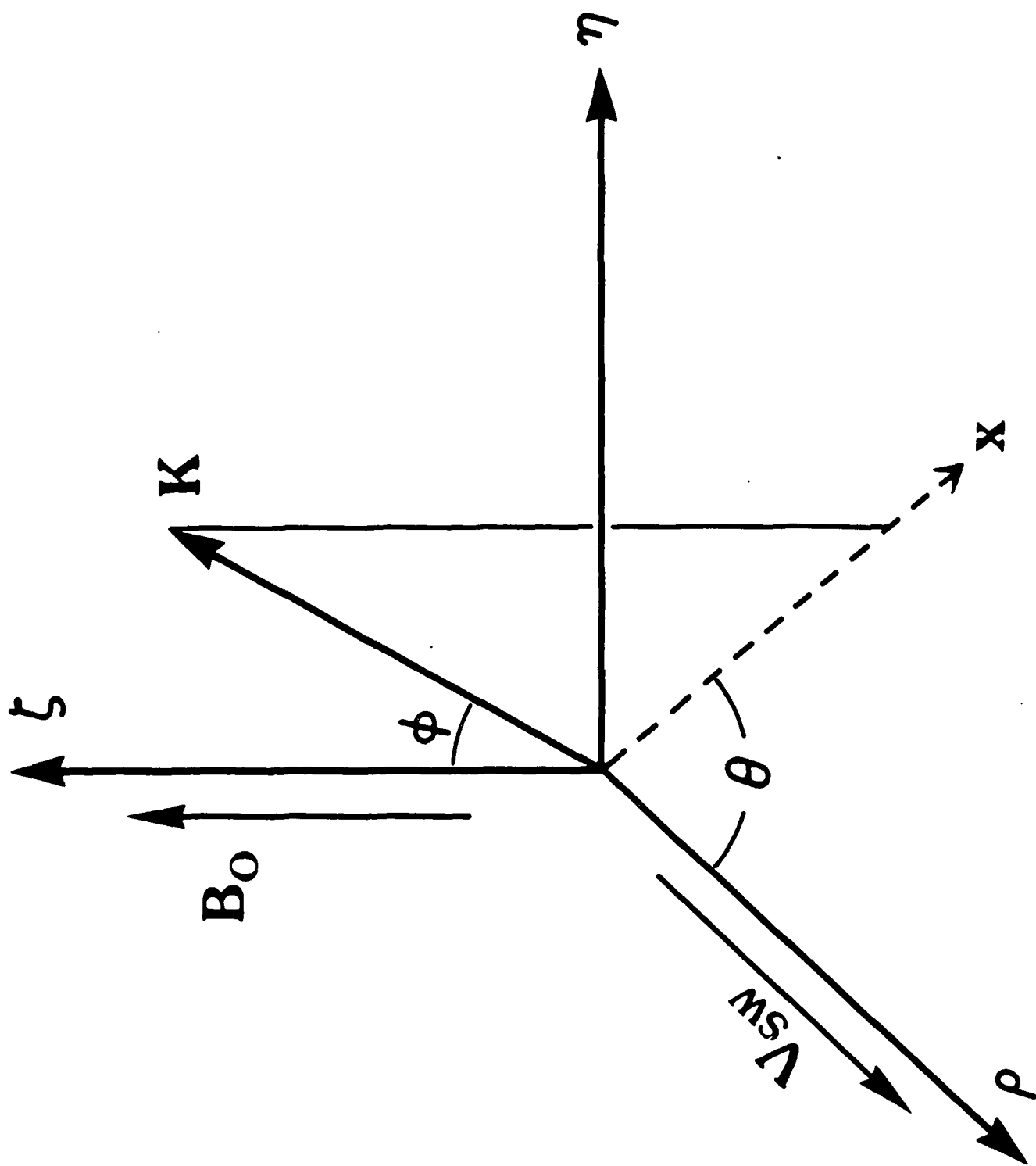


Figure 3

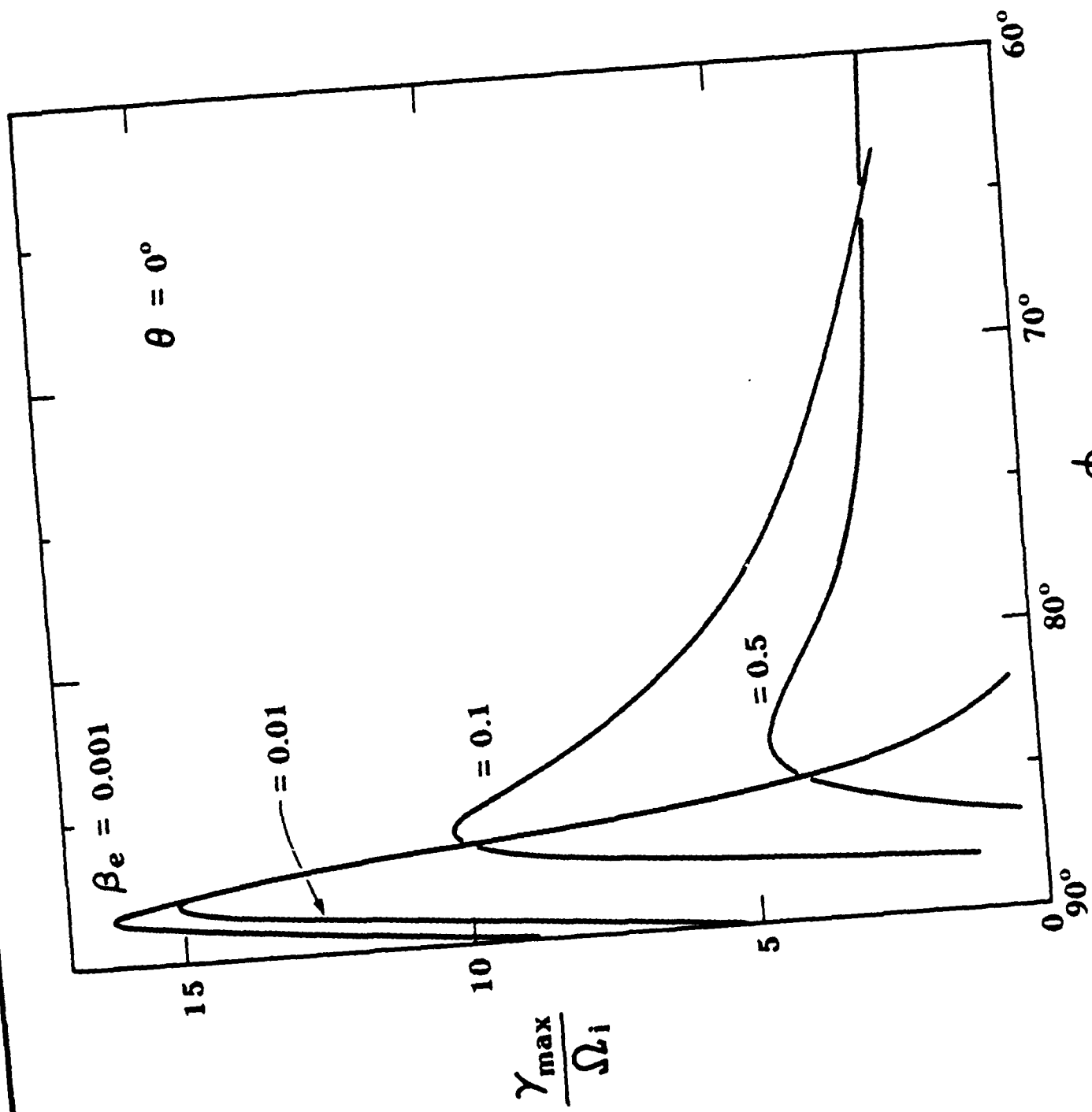


Figure 4

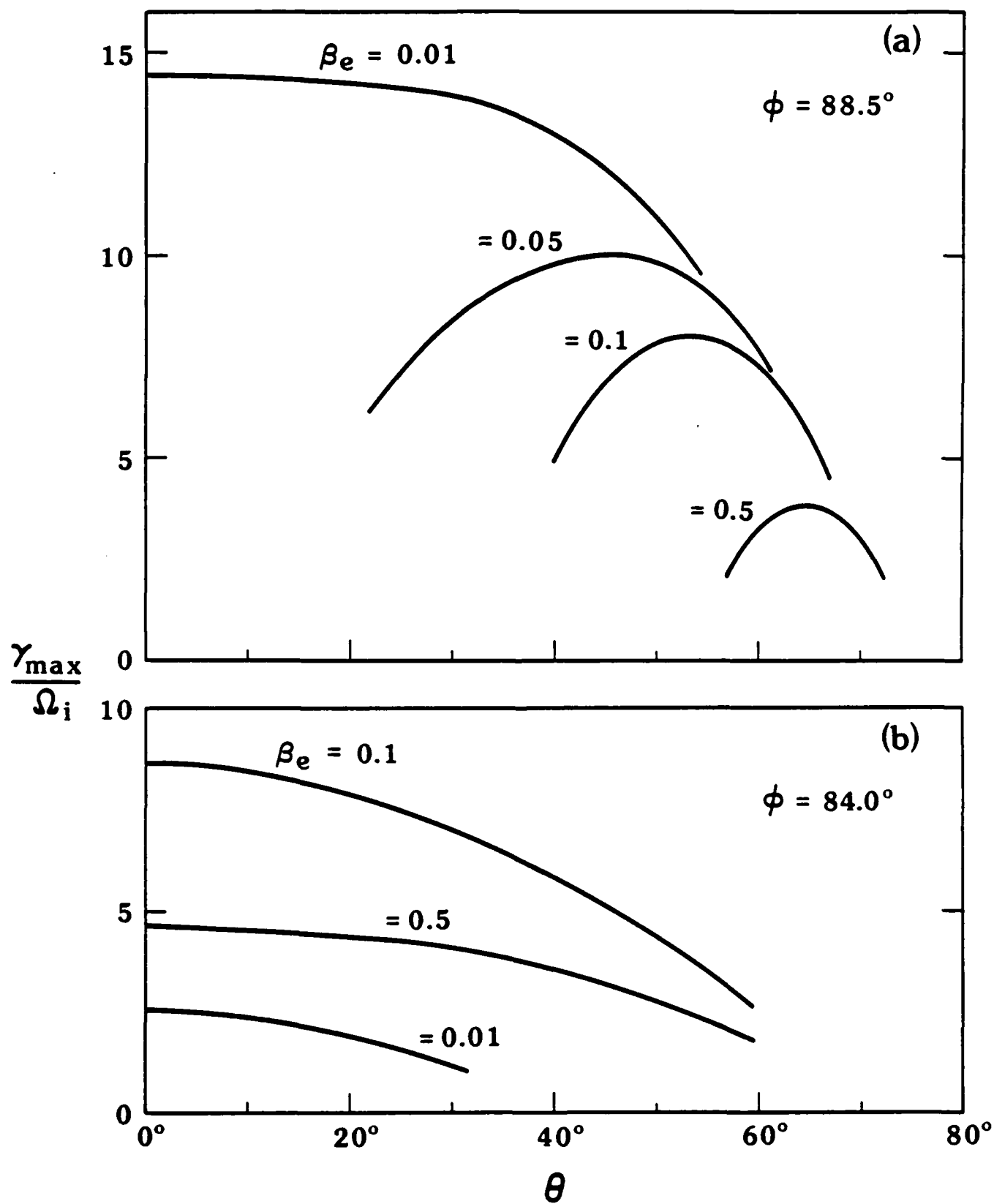


Figure 5

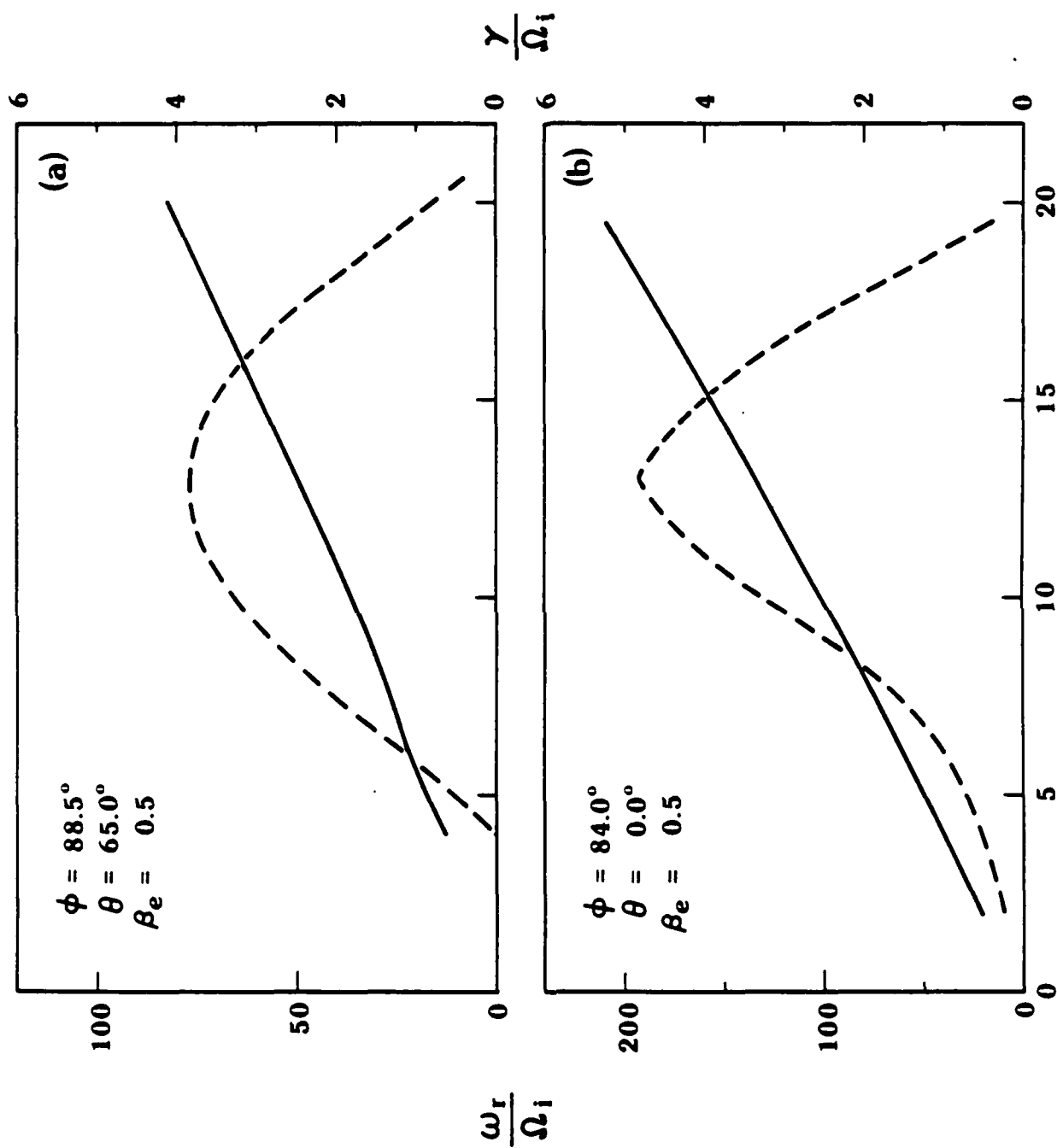


Figure 6

Day 255 1984

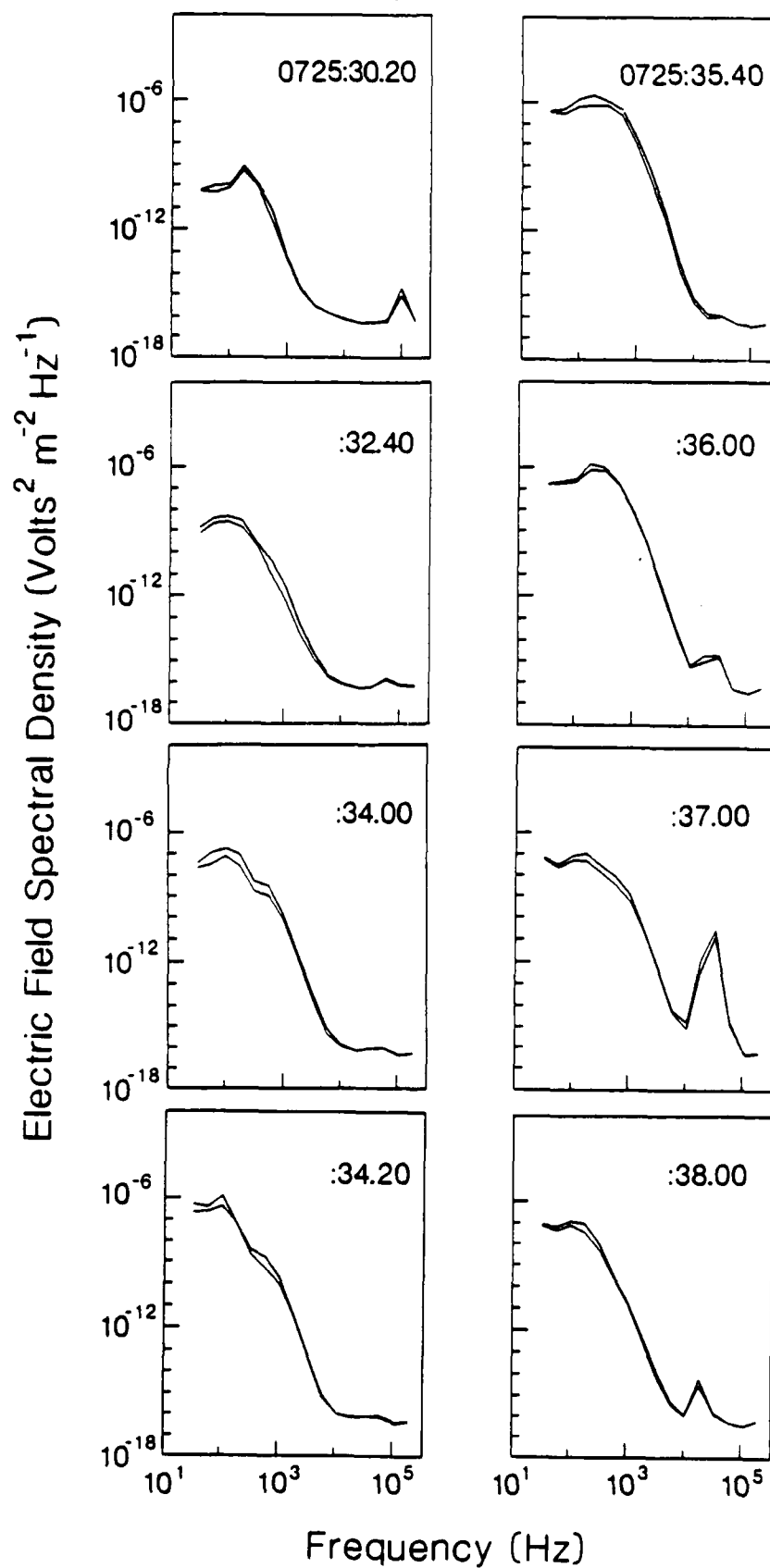


Figure 7

$$N_{\text{Li}} = N_{\text{P}} \quad \theta = 85^\circ$$

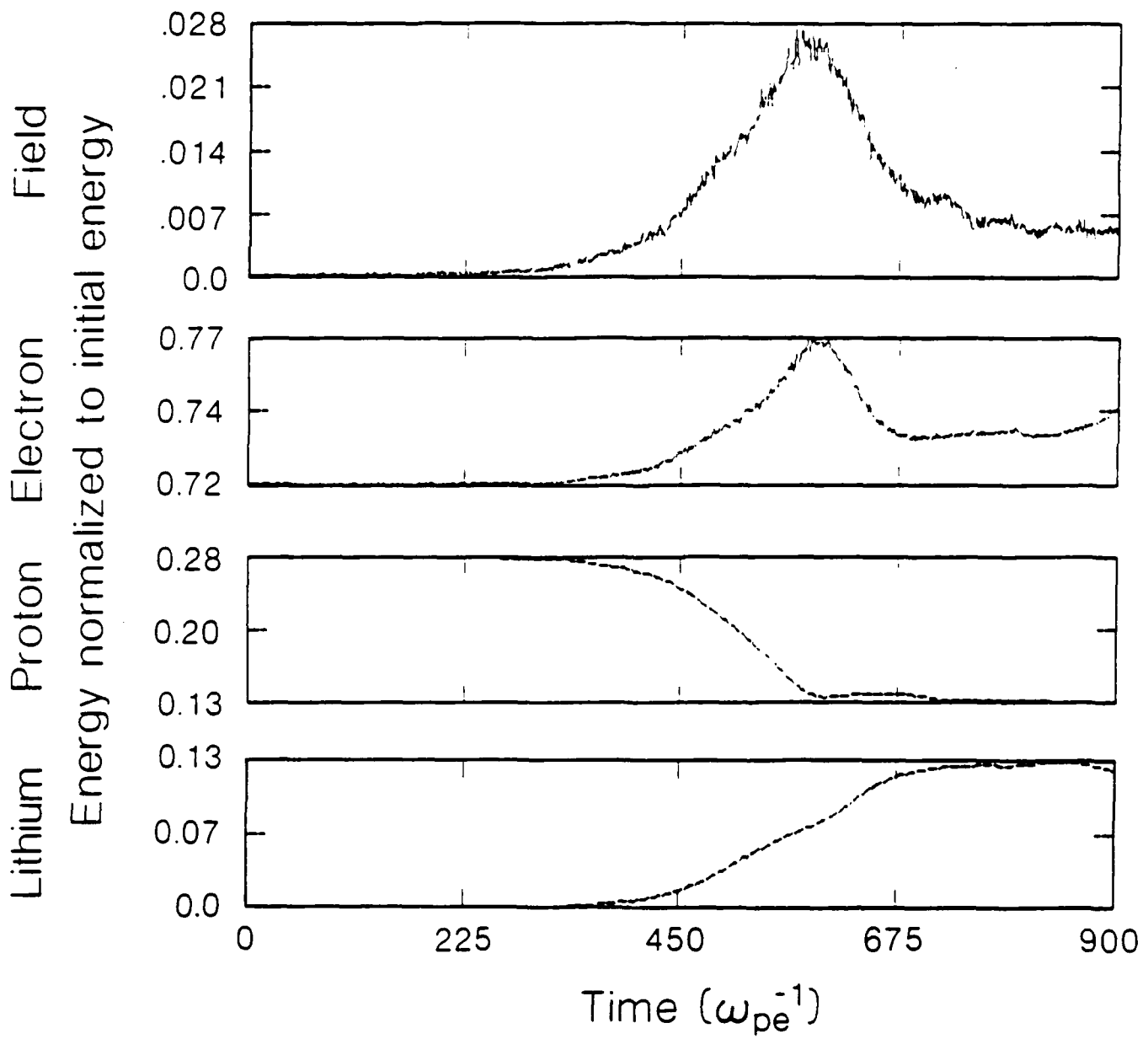


Figure 8

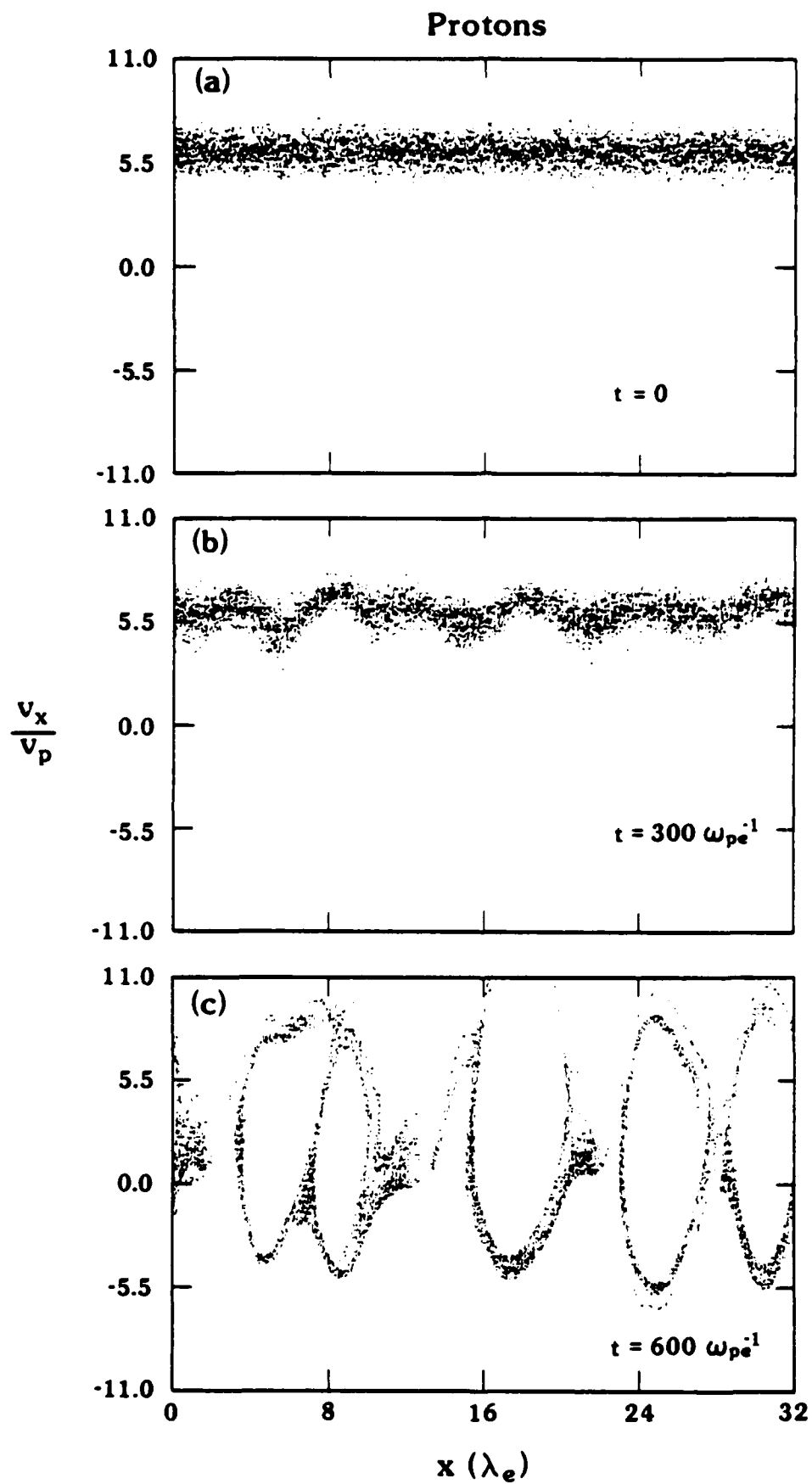


Figure 9

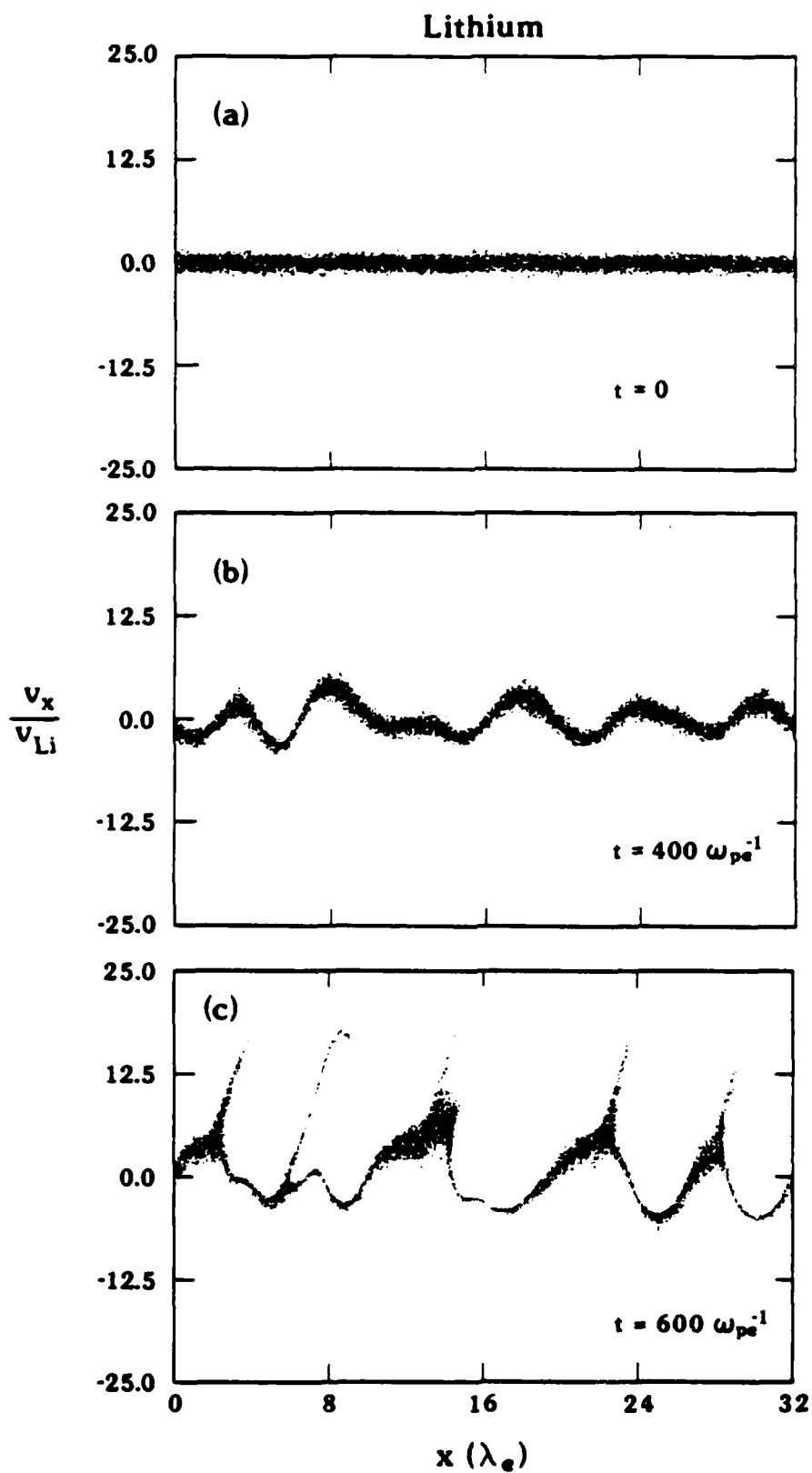
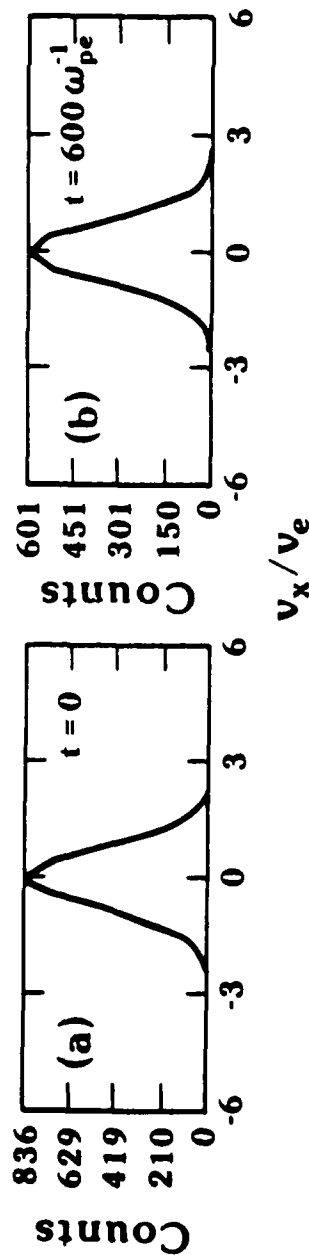
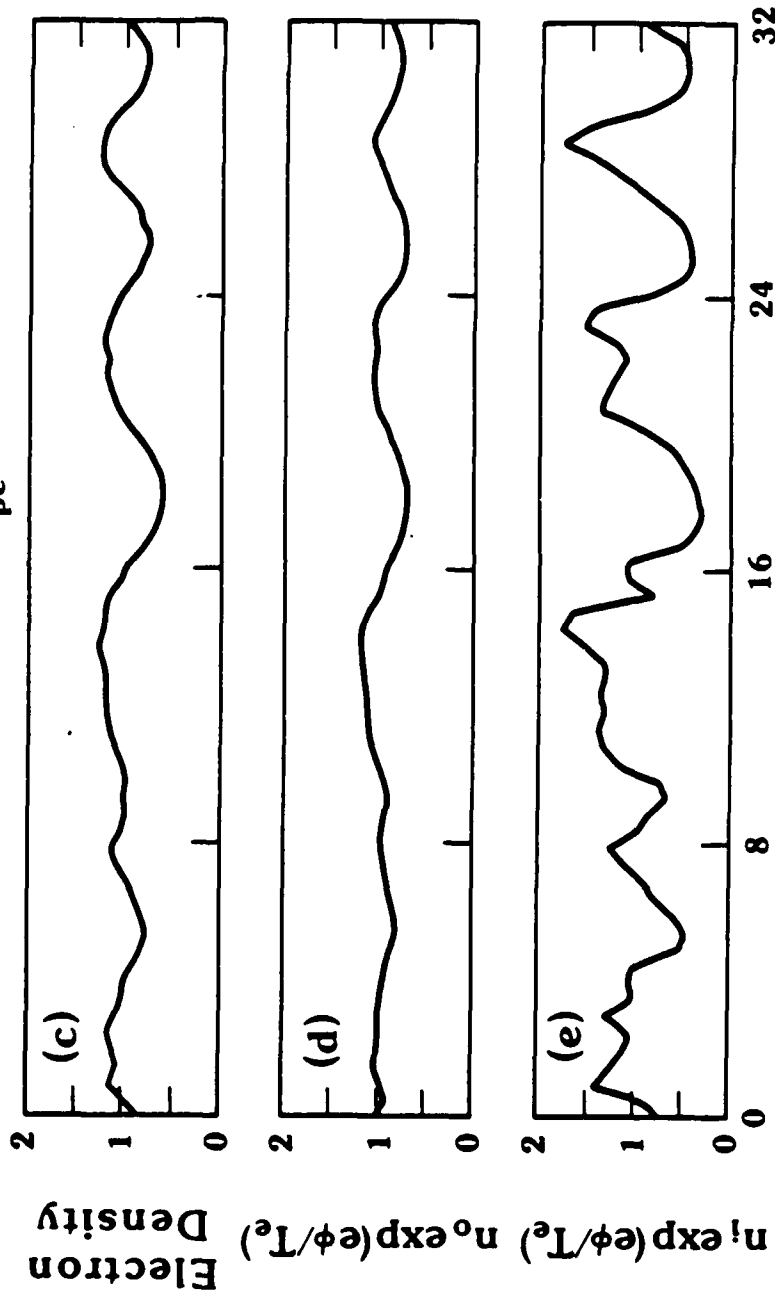


Figure 10

Electron



$t = 600 \omega_{pe}^{-1}$

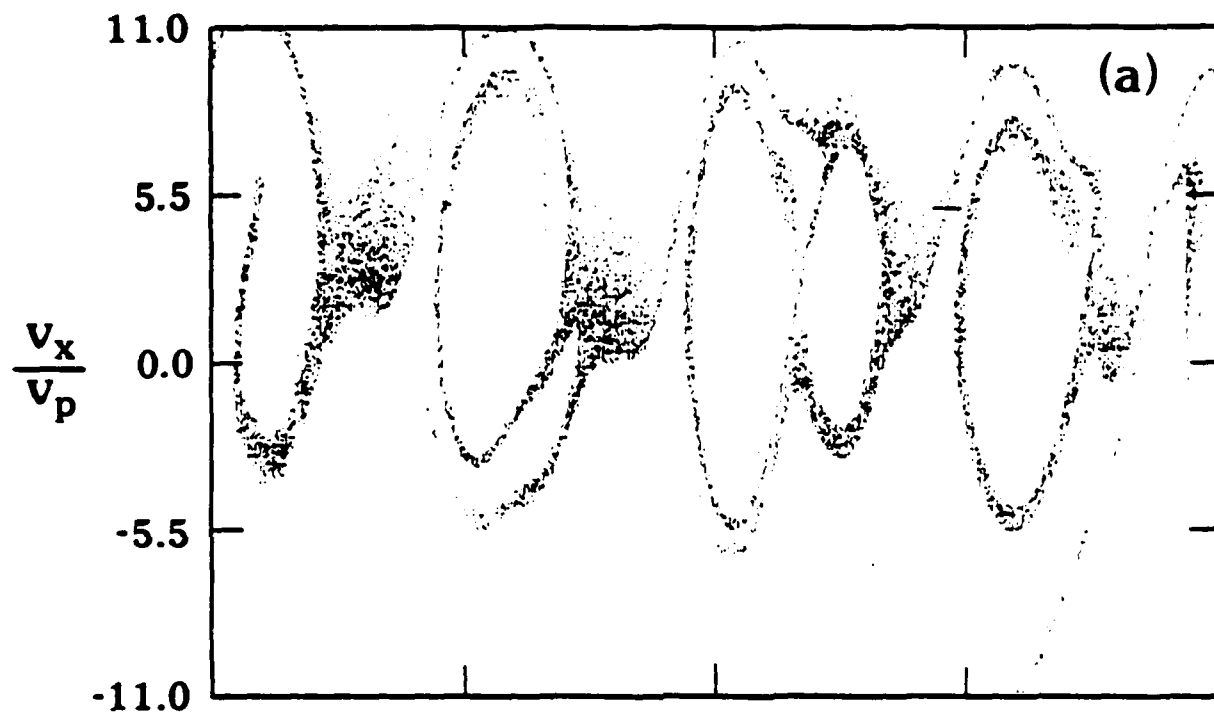


$x(\lambda_e)$

Figure 11

$$t = 600 \omega_{pe}^{-1}$$

Proton



Lithium

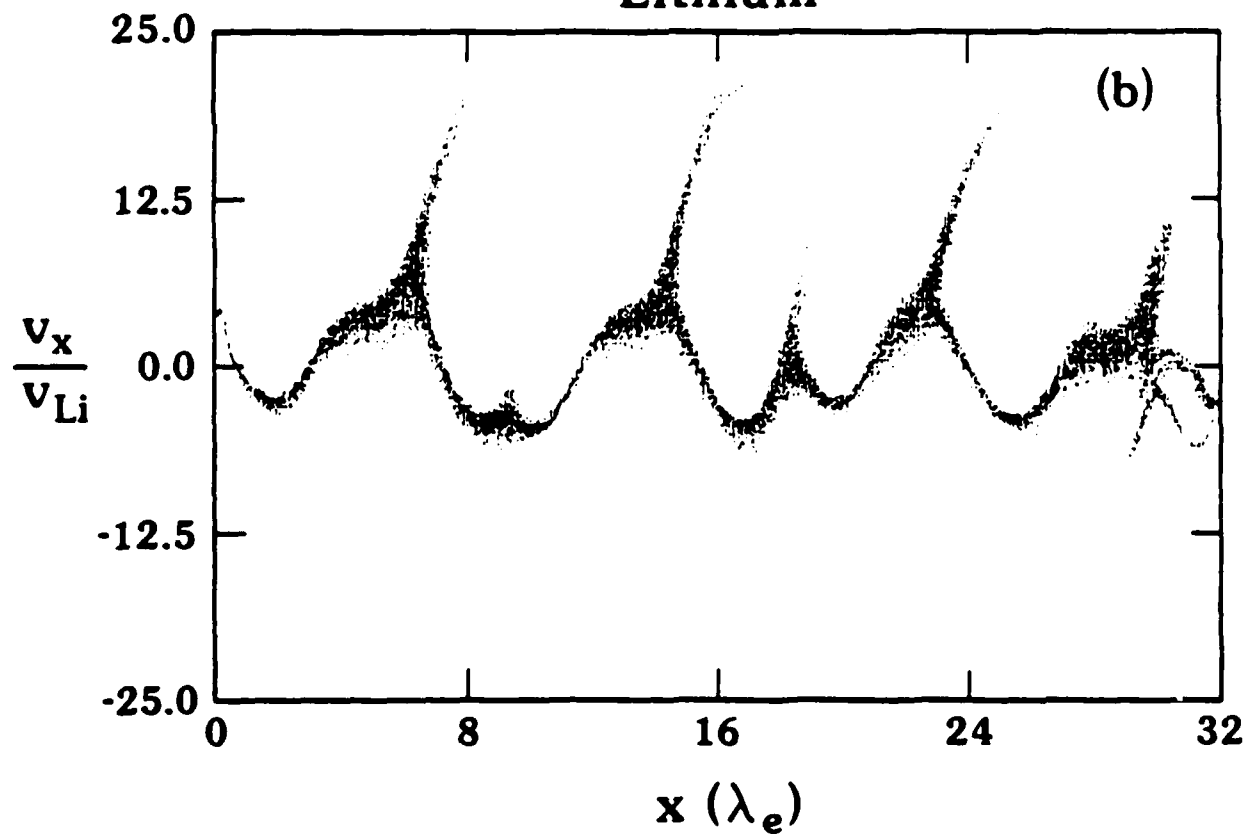


Figure 12

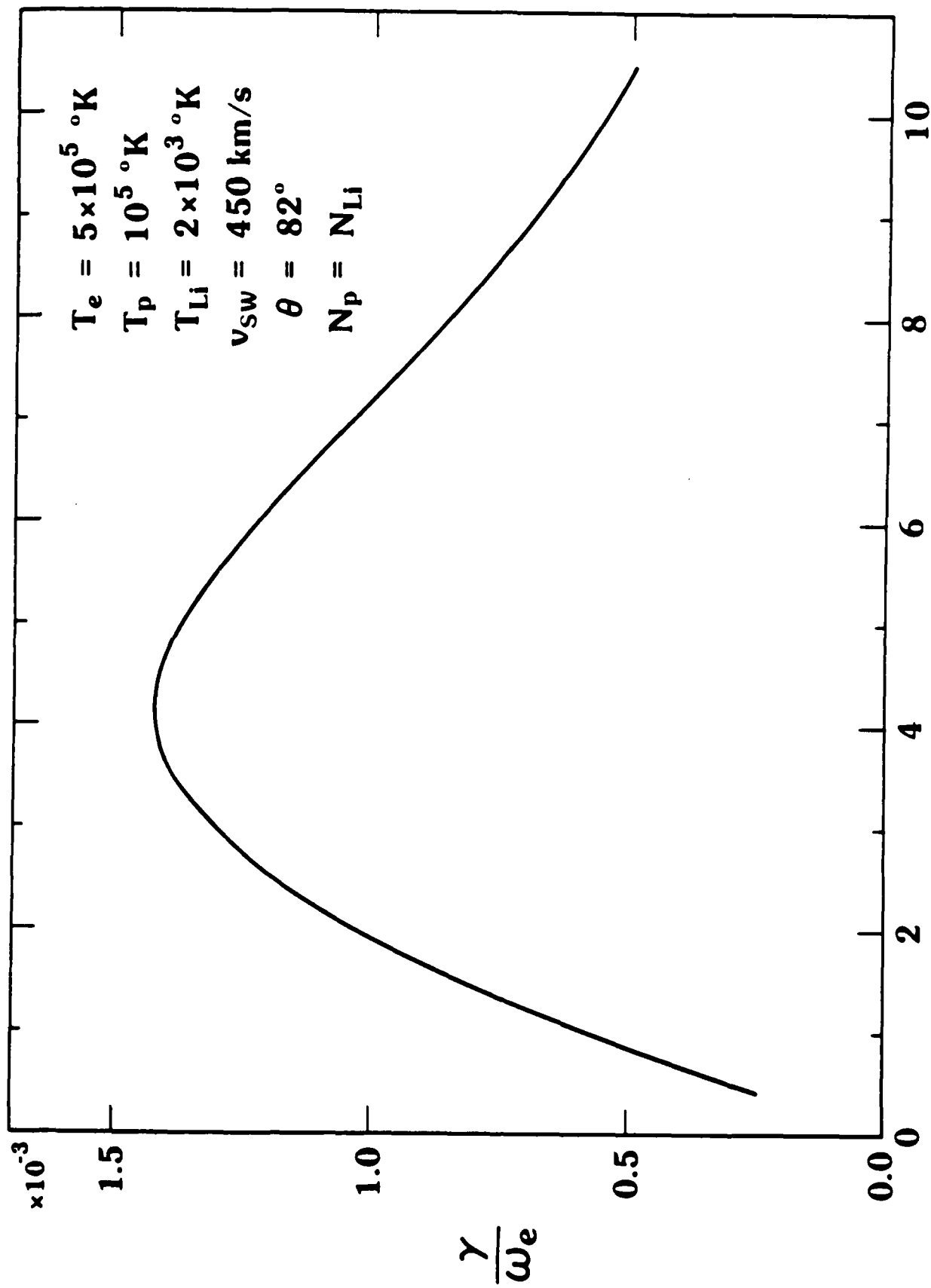


Figure 13

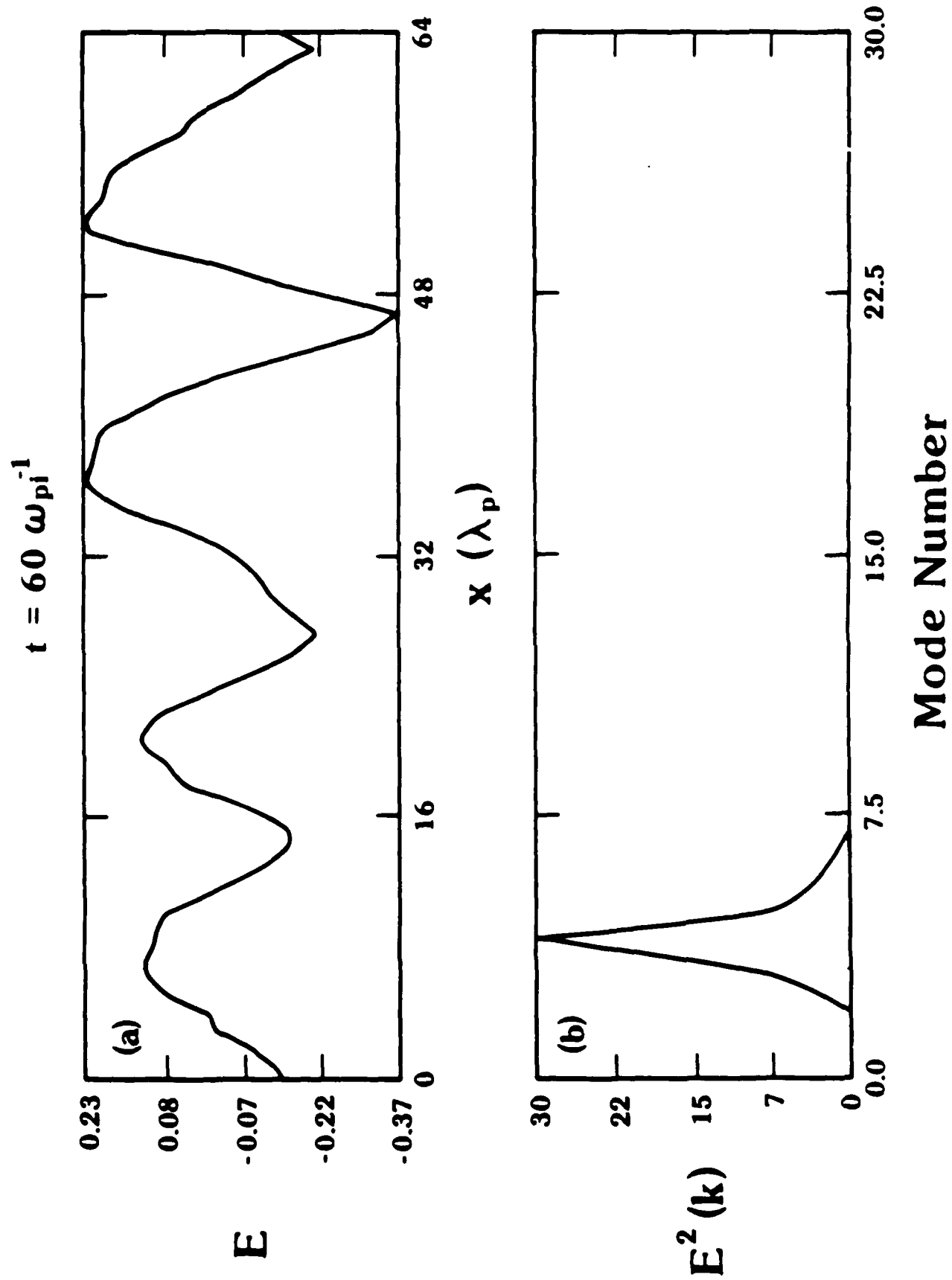


Figure 14

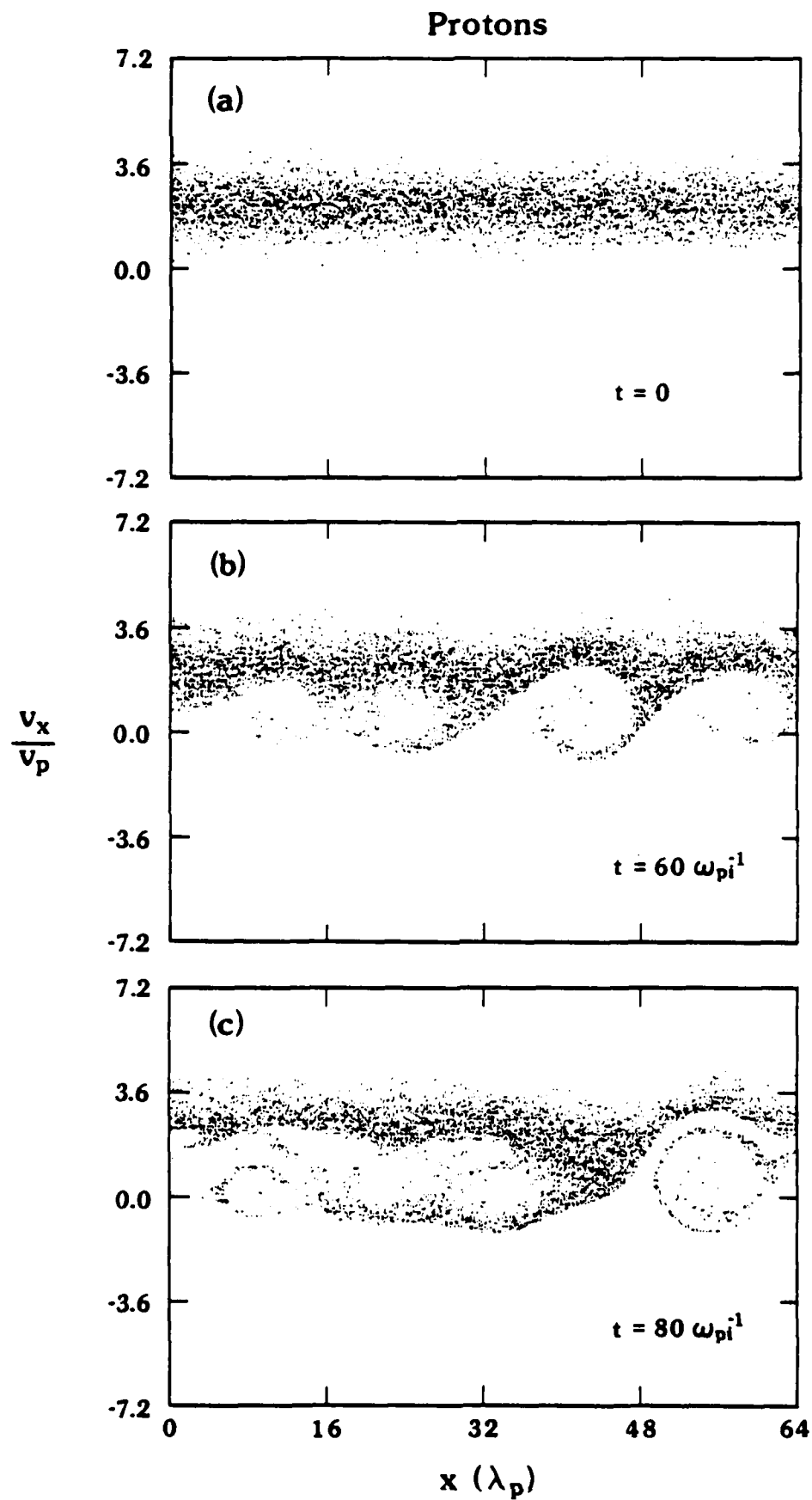


Figure 15

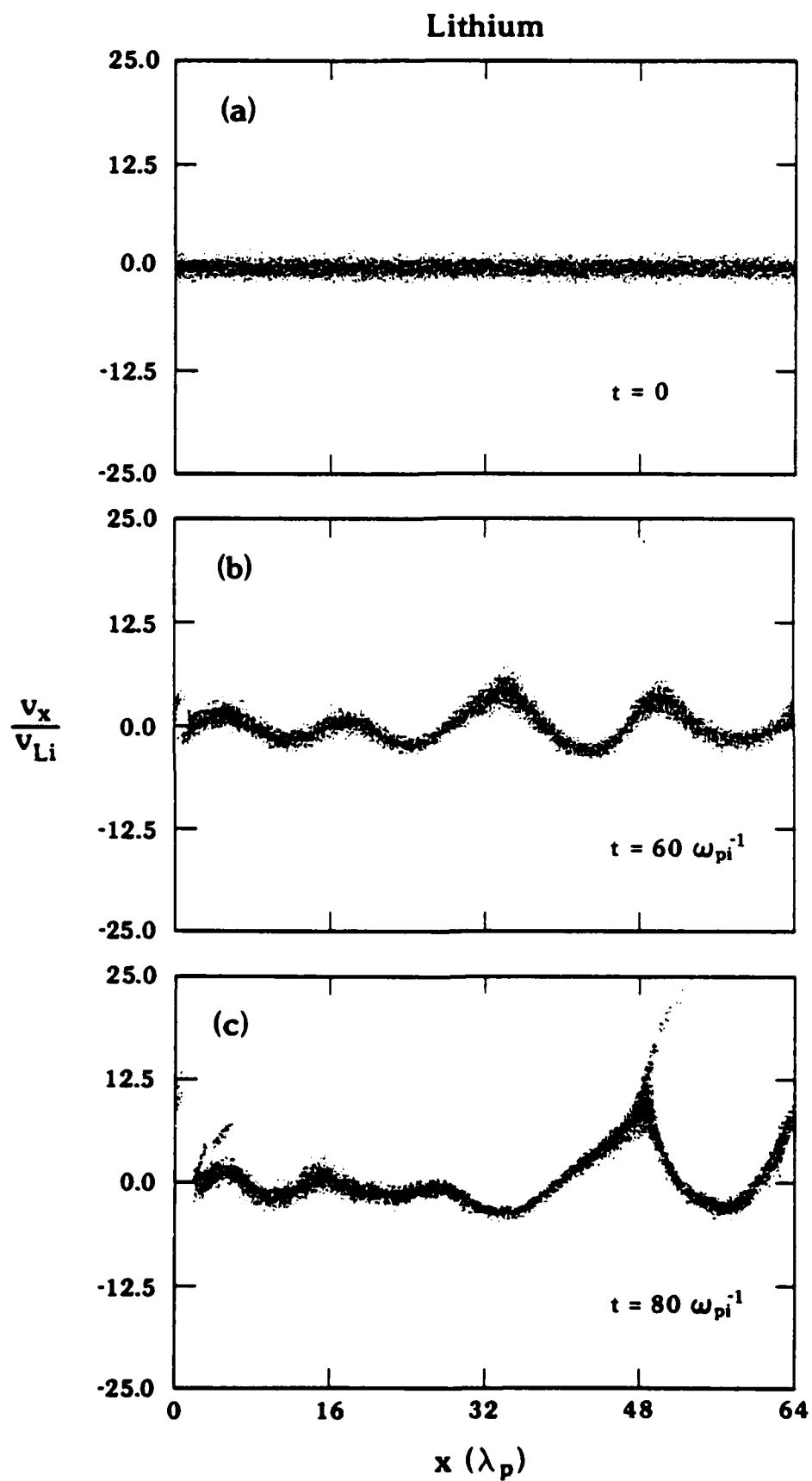


Figure 16

- PPG-1064 "The Focusing of a Relativistic Electron Beam Using a Preformed Ion Channel", S. Wilks, J.M. Dawson, and T. Katsouleas, submitted to Phys. Rev. A, April 1987.
- PPG-1065 "On MHD Intermediate Shocks," C. C. Wu, to be published to Geophys. Res. Letts., May, 1987.
- PPG-1066 "Development of a Mass - Sensitive Ion Energy Analyzer" G. Hairapetian and R. Stenzel, submitted to R.S.I. May, 1987.
- PPG-1067 "The MHD Intermediate Shock Interaction with an Intermediate Wave: Are Intermediate Shocks Physical?" by C. C. Wu, May, 1987.
- PPG-1068 "Linear Instabilities in Multicomponent Plasmas and their Consequences on the Auroral Zone" D. Schriver and M. Ashour-Abdalla submitted to J.J.R., May, 1987.
- PPG-1069 "Cosmic Ray Acceleration: A Plasma Physicist's Perspective" C.F. Kennel, submitted to Inter. "Rosenbluth Symposium", on Dynamics of Particles and Plasmas, Austin, Texas, February 5-6, 1987.
- PPG-1070 "Ray Tracing Analysis of LH Fast Waves in CCT", T.K. Mau, K.F. Lai, R.J. Taylor, submitted to the 7th APS Conference, Kissimmee Florida, May 4-6 1987.
- PPG-1071 "Combined Wiggler and Solenoidal Field Effects In Free Electron Laser and Electron Cyclotron Maser," T. H. Kho and A. T. Lin, invited paper presented by A. T. Lin at the Fourth International Symposium on Gyrotron and Free Electron Laser, Chegdu, People's Republic of China, May, 1987.
- PPG-1072 "MHD Flow in a Curved Pipe," F. Issicci, N.G. Ghoniem, and I. Catton, submitted to Phys. Fluids, June 1987.
- PPG-1073 "The New Roles of Cavitones in Inhomogeneous Plasmas Under Strong Electromagnetic Irradiation" T. Tanikawa, Ph.D Dissertation.
- PPG-1074 "Progress Report on Pisces: Plasma-Surface Interactions and Materials Research" Pisces Group *R. W. Conn, D. M. Gobel, Y. Hirooka, B. LaBombard W. K. Leung and R. Nygren. June, 1987.
- PPG-1075 "Self-Consistent Modification of a Fast Tail Distribution by Resonant Fields in Nonuniform Plasmas," G. J. Morales, M. M. Shoucri and J. E. Maggs, submitted to Phys. of Fluids, June, 1987.
- PPG-1076 "Theory and Simulations on Beat Wave Excitation of Relativistic Plasma Waves," W. B. Mori, Ph.D. dissertation, June 1987.
- PPG-1077 "Equilibrium and Wave Properties of Two-Dimensional Ion Plasmas", G.J. Morales and S.A. Prasad, submitted to Phys. of Fluids, June, 1987

- PPG-1078 "Observation of Stable Axisymmetric Mirror Equilibrium at Arbitrary β ", A. Kuthi, H. Zwi, L. Schmitz and A.Y. Wong, submitted to Phys. PRL., June 1987.
- PPG-1079 "Stability of a Rotating Field Generated Mirror Equilibrium", A. Kuthi, submitted Phys. Lett. A, July 1987.
- PPG-1080 "Dynamical Computer Simulation of the Evolution of a 1-D Dislocation Pileup", R. Amodeo, and N.M. Ghoniem, submitted Int'l. J. of Engr. Sci., July 1987.
- PPG-1081 "International Collaboration in Theory and Modeling of Radiation Damage in Fusion Materials Utilizing Supercomputers", N.M. Ghoniem, ed., July 1987.
- PPG-1082 "Trip Report - Plasma Physics Division Meeting", Burton D. Fried, Madrid, June 22-26, 1987 .
- PPG-1083 "Nature and the Nonlinear Evolution of Electrostatic Waves Associated With The AMPTE Solar Wind Releases", N. Omid, K. Akimoto, D.A. Gurnett and R.R. Anderson, submitted JGR, June 11, 1987.

END

12-87

DTIC